

Design of Novel Generation of Rigid Revolute, Cardan and Ball Joints

by

© Mohammad Hassan Faghih

A Thesis submitted to the

School of Graduate Studies

In partial fulfillment of the requirements for the degree of

Master of Engineering

Faculty of Engineering and Applied Science

Memorial University of Newfoundland

May 2017

St. John's

Newfoundland

Abstract

The thesis is focused on the design and fabrication of different joints as part of a team member of three master's students to design a parallel robot in the fishery. The general approach of how to design a parallel robot is presented. Then, the design and fabrication of a fully articulated snow crab as a model is given in order to use as a test model for the parallel robot. A new design of the revolute joint with a novel concept is presented in this work. The revolute joint with a conical shape uses two sleeves between the joint parts which are coated with Molybdenum Disulfide (MoS_2). The role of MoS_2 is to lubricate the inner parts of the revolute joint. A method for choosing the taper angle is presented based on the application. The authors fabricated the proposed new design at the machine shop of Memorial University and the joint proved to have successful functionality. Afterwards, the design and fabrication of the fork revolute joint, cardan joint (universal joint) and ball joint based on the design of the revolute joint is represented. Overall, the design of different joint types in this thesis is usable not only in the parallel robot but also in many mechanisms and applications.

Acknowledgements

I would like to express my sincere gratitude to my supervisor, Dr. Luc Rolland, for his motivation, encouragement, assistance and support throughout my program. He has always been a friend and an advisor to me.

I would also like to thank the Research & Development Corporation (RDC) which have provided me with financial support for this program.

I would like to acknowledge Dr. Ali Reza Dehghani, Dr. Saeed Reza Dehghani, Mr. Javad Abedini and Mr. Mehdi Masoodi who have given me excellent technical advices.

In addition, I would like to thank Md. Toufiqul Islam and Shengqi Jian who were great team mates.

I am so grateful to Cheng Yin, my other team mate, who has always been accessible whenever I needed his help.

My gratitude also extends to Dr. Leonard Lye, Dr. Michael Hinchey, Dr. George Mann and Dr. Yuri Muzychka who were my course instructors.

Table of Contents

Abstract	i
Acknowledgements.....	ii
Table of Contents	iii
List of Tables	viii
List of Figures	ix
Chapter 1: Introduction	1
1.1. Background Motivation.....	1
1.2. Thesis Objective	2
1.3. The Contributions of the Thesis	3
1.4. Break Down of Chapters	3
Chapter 2: Background Study.....	5
2.1. Literature Review	5
2.1.1. Revolute Joint	5
2.1.2. Universal Joint	10
2.1.3. Ball Joint	12
2.2. State of the Art	13
2.2.1. Revolute Joints.....	13
2.2.2. Universal Joints.....	13

2.2.3.	Ball Joints.....	14
2.3.	The Applications Where Rigid Rotational Joints Are Needed	16
2.4.	Why and How Robot Designs Can Be Implemented for High Speed Manipulation	
	16	
2.4.1.	Introduction.....	16
2.4.2.	Robotic Manipulators.....	17
2.4.3.	Summary	24
2.5.	Problem Statement	24
2.6.	Coordinate Measuring Machine	25
2.7.	Rapid Prototyping and Manufacturing.....	26
2.7.1.	Stereolithography (SL).....	27
2.7.2.	Binder Jetting	28
2.7.3.	Fused Deposition Modeling (FDM).....	29
2.7.4.	Selective Laser Sintering (SLS).....	30
2.7.5.	The Comparison of RP Methods.....	32
Chapter 3:	Design and 3D Print a Fully Articulated Crab	33
3.1.	The Purpose of This Crab Joint Modeling	34
3.2.	The Joint Models for the Snow Crab	35
3.2.1.	Fork Ball Joint Used in the Back Legs	37

3.2.2.	Revolute Joint for All the Knee Legs.....	38
3.2.3.	Combination of Revolute and Ball Joint Used in the Claw Leg.....	39
3.3.	Prototyping the Snow Crab	40
3.3.1.	Manipulation of the 3D Model in the CAD Program	40
3.3.2.	Producing the 3D Physical Model	41
Chapter 4:	Joint Design.....	45
4.1.	Revolute Joint.....	45
4.2.	Dry Friction	46
4.3.	Conical Joint Optimization.....	47
4.3.1.	Optimization of Simple Planar Case in Vertical Direction.....	49
4.3.2.	Optimization of Simple Planar Case in the Horizontal Direction.....	52
4.3.3.	Optimization of 3D Model Case in Vertical Direction	57
4.3.4.	Optimization of 3D Model Case in Horizontal Direction.....	66
4.4.	Dry Lubricant Selection	67
4.5.	Conical Joint with Two Sleeves	70
4.5.1.	Single Contact Surfaces	70
4.5.2.	Contact Surfaces with One Removable Sleeve.....	70
4.5.3.	Contact Surfaces with Two Removable Sleeves.....	71
4.6.	Self Locking	73

Chapter 5: Manufacturing and Result	75
5.1. Manufacturing	75
5.2. Results and Discussion.....	78
Chapter 6: Verification	80
6.1. Method of Verification.....	80
6.1.1. Method 1 Weight Ratio.....	81
6.1.2. Method 2: Spring Balance.....	82
6.1.3. Method 3: Tilted Plane.....	83
6.1.4. Method 4: Clamping	84
6.1.5. Method 6: Motorized Tribometers.....	85
6.2. Bed Testbed Structure and Results.....	86
Chapter 7: Fork Revolute Joint	93
7.1. Design.....	94
7.2. Manufacturing	97
Chapter 8: Universal Joint	100
8.1. Design.....	102
8.2. Manufacturing	103
Chapter 9: Ball Joint	106
9.1. Design.....	107

9.2. Manufacturing	111
Chapter 10: Conclusion.....	112
10.1. Conclusion	112
10.2. Future Work.....	115
References.....	116

List of Tables

Table 2-1 Comparison between parallel and serial manipulators	18
Table 4-1 Factors affecting the choice of lubricant class	67
Table 4-2 Comparative properties of Molybdenum disulphide, Graphite and PTFE	69
Table 4-3 Values and dimensions of the conical joint	74
Table 6-1 The verification result with ± 1 gram tolerance	89
Table 6-2 The final verification and comparison results	92

List of Figures

Figure 1-1 A wide V plane guideway used in CNC machine made by OKUMA (the courtesy of OKUMA)	2
Figure 2-1 A schematic of the revolute joint	5
Figure 2-2 Philip Vaughan’s (1794) ball bearing for “certain axle-trees, axle-arms, and boxes for light and heavy wheel carriages.”	6
Figure 2-3 Sven Wingquist patent - multi-row self-aligning design of the ball bearing	7
Figure 2-4 Thrust-bearing and like machine element by Michell	8
Figure 2-5 A schematic of the universal joint	10
Figure 2-6 A schematic of the ball joint (courtesy of mathworks)	12
Figure 2-7 A Knuckle Joint from MISUMI INDIA Pvt Ltd (courtesy of MISUMI INDIA)	13
Figure 2-8 The universal joints from Curtis Universal Joint Company with different materials and purposes (courtesy of Curtis Universal)	14
Figure 2-9 The Moog® domed cover plate design used in ball joints, tie-rod ends and socket-style sway bar links (the images have been provided Courtesy of Moog®)	15
Figure 2-10 Hephaist’s spherical rolling joint (courtesy of myostat)	15
Figure 2-11 A serial SCARA robot from Mitsubishi Electric (courtesy of Mitsubishi Electric).....	17
Figure 2-12 A parallel Five-Bar robot from Mitsubishi Electric (courtesy of Mitsubishi Electric).....	18

Figure 2-13 Lufthansa flight simulator on 6-axis platform based on Stewart platform (courtesy of Lufthansa).....	21
Figure 2-14 A planar parallel 3-RPR manipulator fabricated in Ohio University	21
Figure 2-15 ABB Flexible Automation's IRB 340 FlexPicker (courtesy of ABB Flexible Automation)	22
Figure 2-16 CMMs	26
Figure 2-17 A schematic of stereolithography technology (has been provided Courtesy of CustomPartNet Inc)	28
Figure 3-3 A schematic of binder jetting technology (has been provided Courtesy of CustomPartNet Inc)	29
Figure 3-4 A schematic of fused deposition modeling technology (has been provided Courtesy of CustomPartNet Inc)	30
Figure 3-5 A schematic of Selective Laser Sintering technology (has been provided Courtesy of CustomPartNet Inc)	31
Figure 3-6 A schematic of a real snow crab	35
Figure 3-7 The 3D scan model of a snow crab (courtesy of the Marine Institute)	36
Figure 3-8 The fork ball joint used in each back leg	37
Figure 3-9 The sketch of revolute joint for the knees	38
Figure 3-10 The combination of revolute joint and ball joint used in the claw leg	39
Figure 3-11 The fully articulated snow crab model	40
Figure 3-12 RP machines at Memorial University	42
Figure 3-13 Different trials with various tolerances	42
Figure 3-14 The fully articulated snow crab produced by FDM (the scale factor 0.7:1) ..	43

Figure 3-15 The fully articulated snow crab produced by SLS	44
Figure 3-16 The fully articulated snow crab produced by SLS (the scale factor 1:1)	44
Figure 4-1 A schematic of a revolute joint in conical shape.....	46
Figure 4-2 The case in which the direction of gravity is alongside the main axis (Z axis)	50
Figure 4-3 The direction of gravity is perpendicular to the main axis (Z axis) - FBD of outer joint	52
Figure 4-4 Min <i>F_{n,1}</i> at $\alpha = 0.64$ rad or 37°	55
Figure 4-5 Min <i>F_{n,1}</i> at $\alpha = 0.99$ rad or 57°	55
Figure 4-6 Trend ratio of <i>F_{springW}</i>	56
Figure 4-7 The revolute conical joint and the location of reference frame.....	57
Figure 4-8 The free body diagram for outer joint	58
Figure 4-9 A comparison example with assumption of uniform pressure and uniform wear (courtesy of Ambekar A. G.'s book)	63
Figure 4-10 A schematic of the conical joint with external forces	65
Figure 4-11 The full assembly of conical joint with two sleeves	71
Figure 4-12 Exploded view of conical joint with two sleeves	72
Figure 5-1 The conical joint assembly as a rigid revolute joint.....	76
Figure 5-2 The conical joint parts	77
Figure 5-3 The fabricated conical joint installed on the 3-RPR planar parallel robot at the High Performance Robot Lab at Memorial University.....	77
Figure 6-1 Schematic diagram of static frictional test setup - weight ratio method	81
Figure 6-2 Schematic diagram of static frictional test setup - spring balance method	82

Figure 6-3 Schematic diagram of static frictional test setup - tilted plane method	83
Figure 6-4 Clamping the object with high contact pressure (courtesy of toolmonger)	84
Figure 6-5 Multi-Purpose Wear Test System MPW110 Friction and Wear Testing - LPR Global, Inc. (courtesy of uskoreahotlink)	85
Figure 6-6 The bed test structure and the position of the parts from front view	87
Figure 6-7 The bed test structure and the position of the parts from top view	88
Figure 7-1 A schematic of a fork revolute joint (courtesy of mathworks)	94
Figure 7-2 The full assembly of fork revolute joint.....	96
Figure 7-3 Exploded view of fork revolute joint	97
Figure 7-4 The fabricated conical fork revolute joint using sleeves.....	99
Figure 8-1 Universal joints by Belden Universal Co. (courtesy of beldenuniversal)	101
Figure 8-2 The design and full assembly of universal joint.....	102
Figure 8-3 Exploded view of universal joint	103
Figure 8-4 The fabricated universal joint using sleeves	105
Figure 9-1 The design and full assembly of the ball joint	108
Figure 9-2 A larger view of the ball joint (RUR)	109
Figure 9-3 A larger view of the ball joint with extended fork parts (RUR)	110

Chapter 1

Chapter 1: Introduction

1.1. Background Motivation

The main goal of this research is to design a family of revolute joints. This requires to optimize configuration parameters including high rigidity, self-centering, low friction and low backlash. This design then led to development of the ideas for the other rotary joints including fork revolute joint, universal joint and ball joint.

One of the inspiring reasons to choose a specific shape of the revolute joint in this thesis was the prismatic joints in machine-tools (Figure 1-1). They achieve rigidity by increasing the contact surface of the guiding rails while they obtain self-centering by using inclined slides which can often look like V notches on one side of the guiding rail. We can make circular and obtain the same advantages.

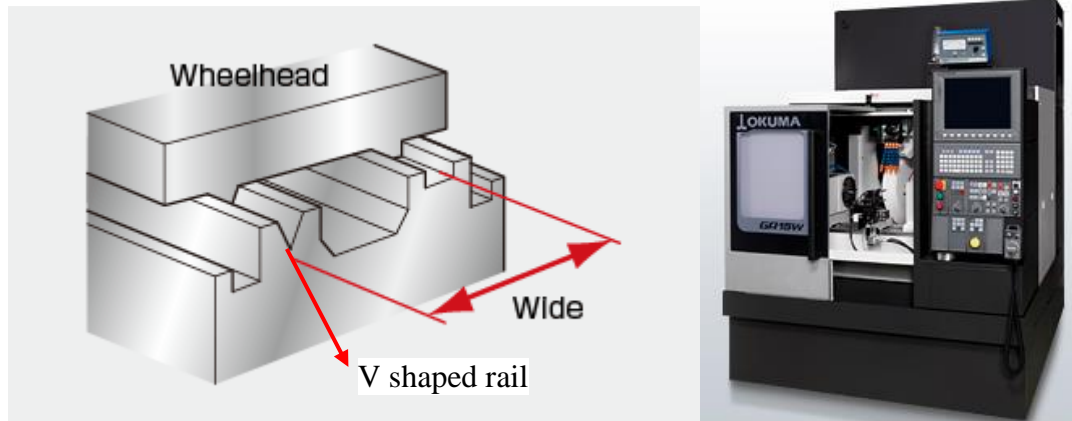


Figure 1-1 A wide V plane guideway used in CNC machine made by OKUMA (the courtesy of OKUMA) [1]

1.2. Thesis Objective

In this research, the author tried to design and manufacture a better revolute joint with desired criteria that can improve the current revolute joint performances and be a good replacement in industry. Consequently, the authors expanded the criteria of the revolute joint design for other types including fork revolute joint, universal joint and ball joint. Eventually, the fork revolute joint and universal joint were fabricated as well as the revolute joint to show the feasibility function of the new joints and appropriate replacements for common joints in industries. Finally, the fabricated revolute joint was replaced with the common ball bearing used in the stand of 3-RPR planar parallel robot at the High Performance Robot Lab at Memorial University to show its successful functionality.

As a result of those efforts, authors could succeed to publish an accepted conference paper [94].

1.3. The Contributions of the Thesis

The thesis considers the design problems of a novel revolute joint. The design criteria include self-centering and self-aligning, low friction, low backlash, high rigidity. This design leads to a conical shape while using two replaceable sleeves and the Moly between them. After design was completed, the rigid revolute joint was fabricated and experimental test was carried out. Then the joint was used in fork revolute joint, universal joint and ball joint applications. The revolute joint was finally used in a parallel manipulator to show its feasibility as a replacement for common revolute joints.

1.4. Break Down of Chapters

Chapter 1 and 2 include the introduction and literature review of three different joints including revolute joint, universal joint and ball joint. Besides, there is an overview in a section of chapter 2 which is investigated on why and how robot designs can be implemented for high speed manipulation of objects such as crabs. At the end of this chapter, a general description of the techniques and methods for CMM and 3D printing is given to show how individual can make a 3D CAD model from an object such as animal and then how it can be fabricated.

In chapter 3, reverse engineering of a real snow crab is carried out by 3D scanning in order to reach a 3D CAD data of the crab and then after, different joints are designed to simulate the movement of crab's legs. The joints are attached to the body of snow crab by

modifying the CAD data and finally the fully articulated crab is fabricated in two different scales by rapid prototyping machines. The goals of this chapter are:

- To design a combination of different joints as well as each one alone
- A physical model of snow crab with all joints and details for robot design purposes such as pick and place the crab by the robot's end-effector as the real one would create hygiene issues
- An idea for the following research to inspire the design a revolute joint, fork revolute joint, universal joint and ball joint with a novel concept

After discussion about the design and fabrication of the snow crab model, the author focuses on design and fabrication of different joints as parts of the parallel robot. The main effort of the author dedicated to design the revolute joint coming in chapter 4 and then manufacturing and verification of the results afterwards. The idea of the other joints design is based on the result of revolute joint design.

Since the design of different joints was done by author as part of a parallel robot working in fishery, designed by other team mates, the robotics and fishery application are not the only goals of the joints design and having multi-purposes attitude is carefully considered.

The name of the published conference paper as a result of current work come into reference chapter for further information.

Chapter 2

Chapter 2: Background Study

2.1. Literature Review

2.1.1. Revolute Joint

One of the common joints used in robotics and also in many industrial applications is the revolute joint, R, which has one degree of freedom and can be rotated on a single-axis. Therefore, the two paired elements of the revolute joint can be rotated about an axis with respect to each other [2] (Figure 2-1). It can also be called a hinge joint or pin joint [3]. Revolute joints can be simply fitted with conventional bearings [4]. There is a wide variety of applications using this kind of joint such as bending mechanisms and door hinges, for example.

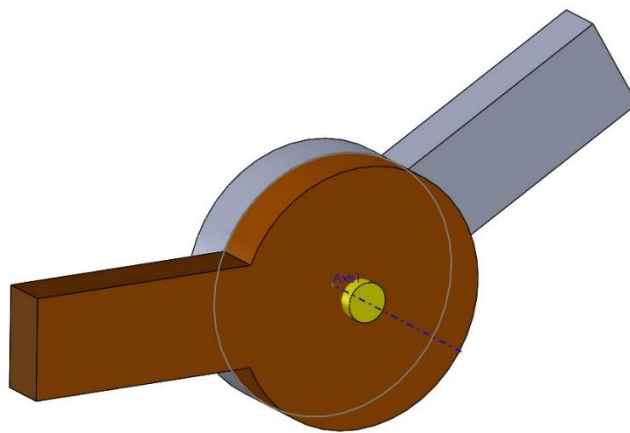


Figure 2-1 A schematic of the revolute joint

Designing and producing a better revolute joint which benefits from the below factors has always been a great source of debate [4-15]. These factors are:

- a) Self-centering and self-aligning
- b) Minimizing friction
- c) Minimizing backlash
- d) Maximizing rigidity

There have been many different and unique revolute joints designed for different applications. The designs of revolute joints have been focused on different parameters such as the shape of the bearings, lubrication, clearance, materials and dynamic analysis.

When there is discussion about bearings, ball bearings are the first and the most famous type which comes to mind. In 1794, Philip Vaughan from England patented the first modern ball bearings [5].

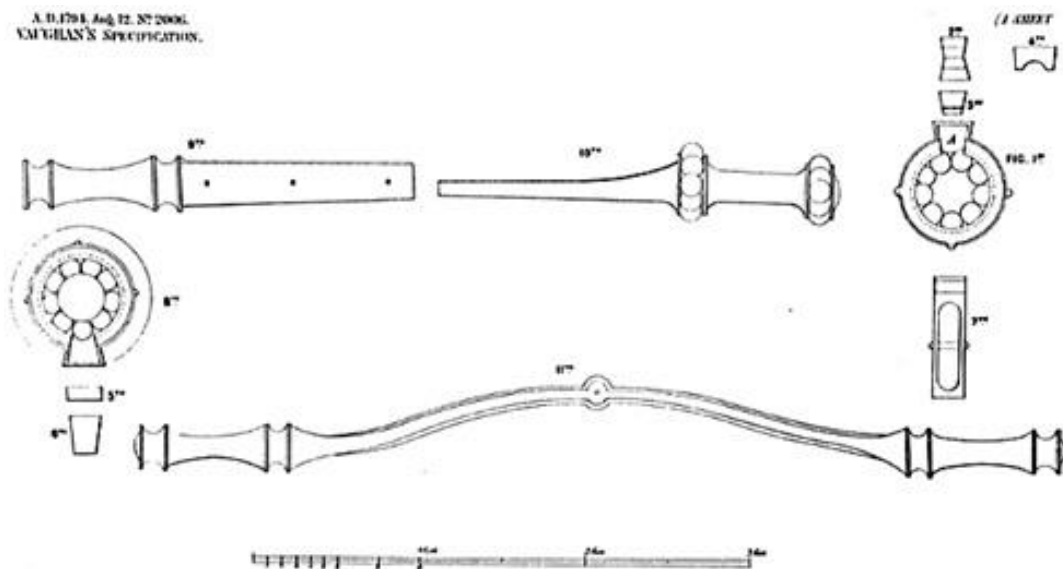


Figure 2-2 Philip Vaughan's (1794) ball bearing for "certain axle-trees, axle-arms, and boxes for light and heavy wheel carriages." [5]

Later, Jules Suriray, a Parisian bicycle mechanic, patented a radial style ball bearing in 1869 [6]. In 1883, Friedrich Fischer, founder of FAG (Fischers Aktien-Gesellschaft), improved a way to produce equal size balls and a round shape for bearings by use of machines [7]. In 1907, Sven Wingquist invented the modern and multi-row self-aligning design of the ball bearing (Figure 2-3) [8].

In the 19th century, the design of bearings and joints was slowly improving while the designers were more focused on some details of the design such as using different materials in production of bearing parts, type of lubricant and later on, more specialized aspects such as dynamic analysis or simulating the behaviour of joints inside the mechanism using relevant software were investigated.

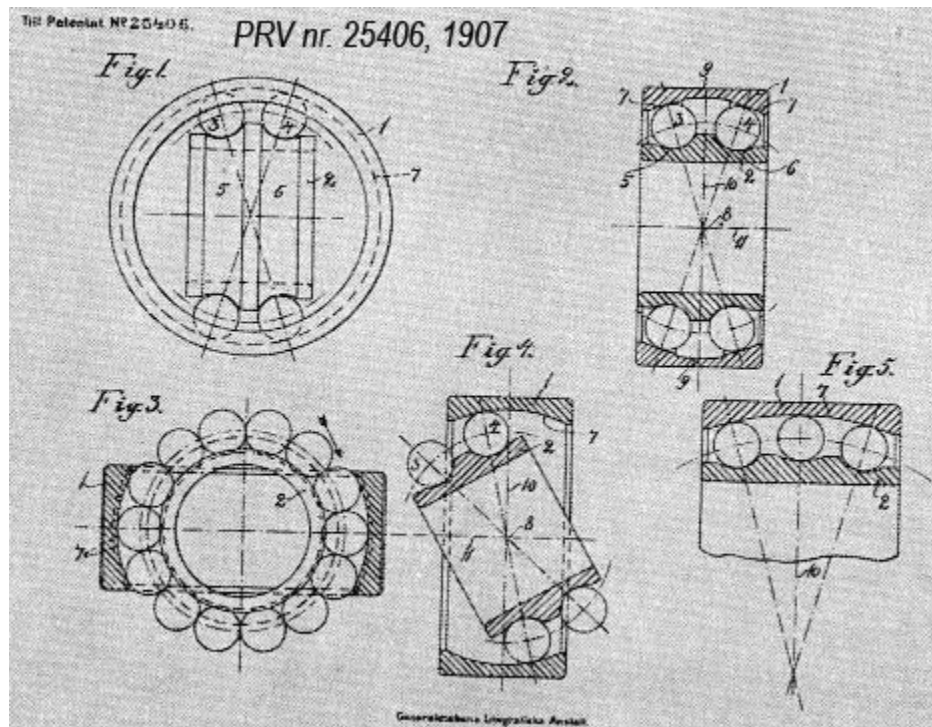


Figure 2-3 Sven Wingquist patent - multi-row self-aligning design of the ball bearing [8]

Michell invented revolute joints containing a number of sector-shaped pads located between the pivoted joint parts. Michell's design eliminated metal-on-metal rubbing by utilizing wedge-shaped regions of oil inside of the joint [9]. The method which is known as pressure-film lubrication refers to hydrodynamic bearings.

There have been many works on hydrodynamic bearings, for instance Bouyer measured the torque with experimental methods on hydrodynamic bearings [10]. He also studied the stick-slip phenomenon at start-up and also the influence of revolute joint characteristics on the friction coefficient.

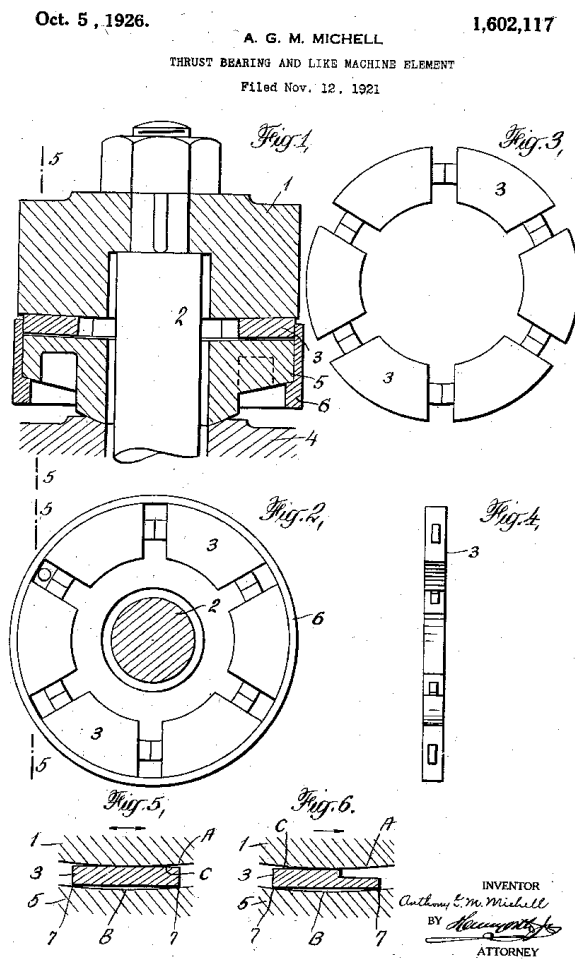


Figure 2-4 Thrust-bearing and like machine element by Michell [9]

Regarding the clearance, Shaoze Yan presented a model for revolute joints considering clearances [11]. Flores carried out the theoretical analysis of revolute clearance joints with and without lubricant consideration [12], [13].

Qiang Tian modeled lubricated cylindrical joints by assuming that there is always lubrication between the journal and the bearing [14].

Zheng Feng Bai and his colleagues introduced a hybrid contact force model of the revolute joint with the combination of the Lankarani–Nikravesh model and the improved elastic foundation model. The model can predict the dynamic behavior of the revolute joint mechanism. It shows the acceleration of the mechanism with clearance results in shaking and a higher oscillation of the mechanism [15].

Keiji Yonemoto designed and fabricated a new flexure revolute joint with leaf springs. The range of motion of their revolute joint is limited although they proposed the design achieving a large range of motion (at least 90 degrees) and a large stiffness ratio. However, the position repeatability and stiffness of the fabricated joint did not reach their calculation expectations [16].

Overall, many designs and investigations in revolute joints have dealt with lubrication and clearances which lead to vibration and oscillation of the mechanism. On the other hand, modeling the joints without considering clearances is easier [17]. Therefore, designing a mechanism with sufficient lubricant and zero-clearance is of a great significance.

2.1.2. Universal Joint

A universal joint, RR, is a joint with 2 rotational degrees of freedom in which the torque or power can be transferred from one shaft to another shaft [18]. Figure 2-5 shows a simple universal joint including two Y-shaped yokes and shafts called driving yoke and driven yoke. Universal joint can also be called U-joint, Cardan joint or Hooke's joint [18].

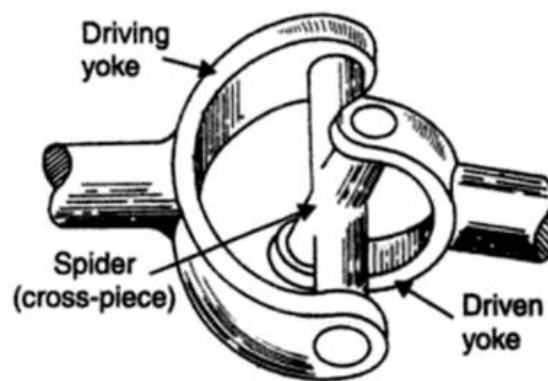


Figure 2-5 A schematic of the universal joint [18]

Because of the nature of the universal joint, the amount of velocity between driving shaft and driven shaft is not constant when they are not along the same axis [18]. It varies as a function of the angle between the shafts.

There are some parameters having negative effects on the output and lifetime of the universal joint such as vibration, backlash, friction and low rigidity among joint parts and finally lead the joint to fail. Over time, different works, designs and investigations have been done to improve the universal joint.

The early investigations on the first joints comes back to Geronimo Cardano in 1550 [19]. After a while, the suspension and the joint that Cardano designed was named “cardan

suspension” or “cardan joint” [19]. In 1667-1675, Robert Hooke analysed the universal joint and proved that the speed of rotation between 2 shafts are non-linear [91].

In order to improve them, some studies and optimization have been carried out. The universal joint torques applied to automobile engine driveshaft to transmit power were analyzed by Dodge and Evernden [20][21]. Dual-number quaternion calculations for four-bar universal joint were performed by Yang and Freudenstein [22]. Freudenstein and Fischer used dual numbers for universal joints to create input-output relationships including fabrication tolerances [23].

In 1962, Gough who was an automotive engineer commenced using universal joint in complex mechanism and he developed his "Universal Tyre-Testing Machine" [24].

In 1970s, instructions to design of the universal joint was introduced by Wagner and Cooney [25]. And then general guidelines were published by other authors such as Shigley and Mischke [26].

The idea of designing the universal joint in this work has resulted from the revolute joint design in which there is no similar literature in this regard. Universal joints are mostly used on drive shafts to transmit power and torque from one source such as engine to the output such as wheels. In our robotics design case, we do not seek to investigate those applications.

On the other hand, the advent of parallel mechanism designs require often to include universal joints which have to be designed with angular displacement between two rigid bodies in mind and not torque transmission.

2.1.3. Ball Joint

A ball or spherical joint, RRR, is a joint with 3 rotational degrees of freedom [27].

By nature, it features very limited range of movement in all directions [27], of about ± 30 degrees.

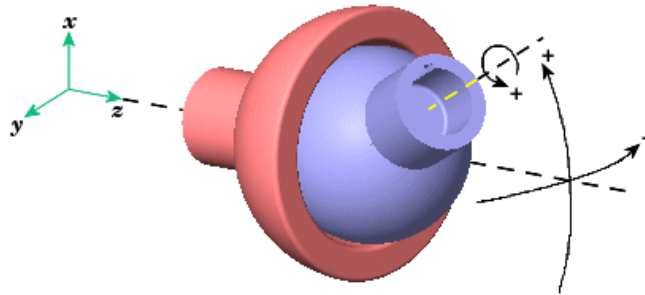


Figure 2-6 A schematic of the ball joint (courtesy of mathworks) [28]

The invention of the ball joint is not very old and it goes back to 1922 when Fritz Faudi patented the ball joint for the automobile industry [29].

In 1972, Jensen Preben W patented a special joint named rolling joint mechanisms [30]. In this mechanism, the three parts transfer the angular motion without sliding friction. Later, more advanced of rolling joint which is called spherical rolling joint are used in industry.

The capability of higher compressive loads, high range of motion and ball-retention are the main factors which have been taken into consideration by designers and experts. However, the results have always been limited particularly in terms of ranges of motion. In this project, the idea of designing the ball joint which evolves from the former joints has been examined.

2.2. State of the Art

2.2.1. Revolute Joints

There are many different designs regarding revolute joints in industry and the common one is shown in Figure 2-7. Therefore, the customers can directly buy a revolute joint from a wide range of standard ones depending on the application. Only rarely, special joints should be designed and manufactured. However, in larger applications, the common revolute joint uses a shaft and a bearing around it which requires lubrication. The joint is attached with a pin (called knuckle joint) [31].



Figure 2-7 A Knuckle Joint from MISUMI INDIA Pvt Ltd (courtesy of MISUMI INDIA) [31].

2.2.2. Universal Joints

Curtis Universal Joint Company is one of the biggest companies in the world which produces different types of joints and mainly universal joints [32]. Figure 2-8 shows the recent products from this company.



Figure 2-8 The universal joints from Curtis Universal Joint Company with different materials and purposes (courtesy of Curtis Universal) [32].

The designs are based on the same joint principle and offer very limited design variety. The company has focused on materials according to their advantages.

2.2.3. Ball Joints

MOOG is one of the production line of Federal-Mogul Corporation which deals with suspension and steering parts [33]. One of the main products they produce is ball joints with high strength and durable performance. Moog® uses a domed cover plate design which can fit into a machined groove [34][35][36][37] (see Figure 2-9). This design offers axial clearances to near-zero backlash, more precise axial and radial deflection consistency than conventional ball joints.

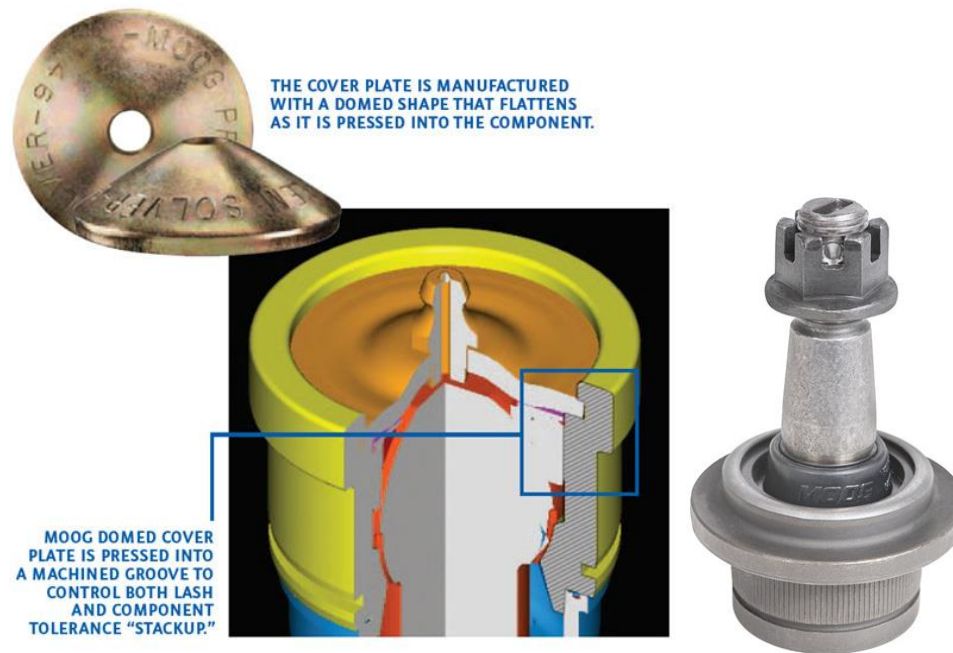


Figure 2-9 The Moog® domed cover plate design used in ball joints, tie-rod ends and socket-style sway bar links (the images have been provided Courtesy of Moog®) [34][36]

Hephaist Seiko in Japan is another company that produces the spherical rolling joints. They claim that low backlash, high rigidity and high precision are the achievements of their products [38]. They feature a double ball joint which are concentric to increase the rotational ranges.



Figure 2-10 Hephaist's spherical rolling joint (courtesy of myostat) [38]

2.3. The Applications Where Rigid Rotational Joints Are Needed

Revolute joints are available in many places and applications. Revolute joints can be seen from wheels, rollers, rotating doors to many big equipment and more complex devices such as serial and parallel robots.

The applications of universal joints, besides the robot industry, are commonly used in automobile's driveshaft although they can be seen in many areas such as aircraft, tool drives or sewing machines [39] [91].

The ball joints are universally used in automobile's suspension [18]. Another type of ball joint called spherical rolling joint is widely used in parallel robotics applications such as the Stewart-Gough [40].

2.4. Why and How Robot Designs Can Be Implemented for High Speed Manipulation

2.4.1. Introduction

In this research, the question has been investigated from a material handling point of view, with specific emphasis on crabs. Afterwards, the suitable type of robot is chosen based on our requirements such as the high acceleration Delta robot [50], or the much simpler planar 3RPR [50], which we have constructed in the High Performance Robotics Laboratory.

2.4.2. Robotic Manipulators

In industry, there are two main categories of robotic manipulators i.e. serial manipulators and parallel manipulators. The main difference is their structure. In serial manipulators, the links and joints are attached together serially beginning from the base extending to the end-effector, hence they have open-ended structures (Figure 2-11). However, in parallel manipulators, the arms are placed in parallel and separately in closed-loop chains, all of which are attached to the fixed base from one side called the fixed base and the mobile platform where the end-effector is located (Figure 2-12) [41].



Figure 2-11 A serial SCARA robot from Mitsubishi Electric (courtesy of Mitsubishi Electric)



Figure 2-12 A parallel Five-Bar robot from Mitsubishi Electric (courtesy of Mitsubishi Electric)

Each type of these manipulators has its own characteristics based on which they may be chosen depending on the needs of the industry. The various characteristics of manipulators are given in Table 2-1.

Table 2-1 Comparison between parallel and serial manipulators [42][43].

	Type of manipulator	
	Parallel manipulator	Serial manipulator
Type of manipulators	Closed loops	Open loop
End effectors	Platform	Gripper

Natural description	In parallel joint space	In serial joint space
Location of actuators	Near the fixed base	On the links
Inertia forces	Less	Higher
Design considerations	Structure, workspace considerations, singularities, link interference	Strength and stiffness considerations, vibration characteristics.
Preferred property	Stiffness	Dexterity
Use of direct kinematics	Difficult and complex	Straightforward and unique
Use of inverse kinematics	Straightforward and unique	Difficult and complex
Singularity	Static	Kinematic
Direct force transformation	Well defined and unique	Not well defined; may be non-existent, unique or infinite
Preferred application	High acceleration	Large reach
Payload-to-weight ratio	High	Low
Work volume	Small	Large

Two popular parallel manipulators are the Gough-Stewart platform (six degrees of freedom), (Figure 2-13), and Delta robot (four degrees of freedom), (Figure 2-15) [44]. Some of the applications of the Gough-Stewart mechanisms are flight simulators, telescopes and underwater research. On the other hand, Delta robots are good at picking, packing and palletizing tasks (pick-and-place) as seen in the food industries. The end-effector of the Delta robot is capable of moving fast in x, y, z axes and rotating around a vertical axis [45]. Recently, Delta robots have been utilized in 3D printers which are a sub-category of rapid prototyping method [46]. Besides, the Adept Quattro™ parallel robot that resembles the Delta robot are used for large work envelope with smooth motion [47]. In addition, for the lighter weight limitation, the simpler planar 3-RPR parallel robots can be preferred [48] (Figure 2-14).



Figure 2-13 Lufthansa flight simulator on 6-axis platform based on Stewart platform (courtesy of Lufthansa) [49]

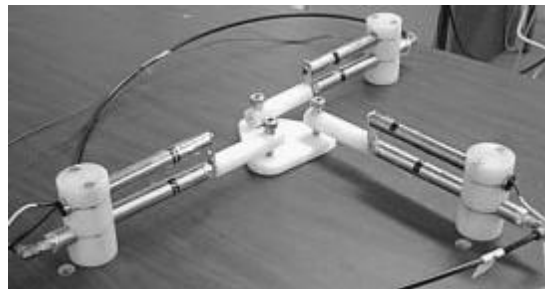


Figure 2-14 A planar parallel 3-RPR manipulator fabricated in Ohio University [48]

In this research, parallel robots have been chosen for material handling manipulation with the following characteristics [50]:

- High speed (both velocity and acceleration)
- High accuracy
- High loading capacity
- High stiffness



Figure 2-15 ABB Flexible Automation's IRB 340 FlexPicker (courtesy of ABB Flexible Automation)

The above mentioned characteristics in parallel robots are resulting from their architecture (Table 2-1). In contrast to serial manipulators, the heavy actuators in parallel robots can be placed in the base, hence the arms can move quickly without carrying the manipulators. Moreover, the arms can theoretically compensate other arms inaccuracies,

whereas in serial robots, the inaccuracy of each arm is added to the others and will finally be transferred to the end-effector.

Parallel robots are more rigid in comparison with serial robot [51]. It may be considered that parallel robots should be more precise since they are more rigid but Bonev and Briot questioned this assertion [52]. Briot and Bonev worked on the comparison between two pairs of serial parallel 2-DOF planar robots and they found out that serial robots are more sensitive to input errors rather than parallel robots [52]. Besides, one of the reasons that the parallel robots lacks high accuracy is the fact that their revolute or universal joints are not rigid enough and have backlash [53].

Now, the parallel robot rigidity comes from the rigidity of the revolute, universal and ball joints which are prone to the following problems: backlash, construction imperfections, low rigidity bearings, not self centered, worst behavior after wear and tear; and these may have a negative impact on overall mechanism rigidity which in turn will worsen accuracy [54].

There were trials to implement the Gough platform (hexapods) as milling machines. However, to this date, there are no such machines in the market capable to achieve precision machining. One of the reasons may well be that the ball and universal joints are relatively flexible. The existing machines can only be used for roughing [55].

In this research, we work with the simpler 3-RPR which has not reached its maturity yet since several design questions were not answered and one of them is building rigid revolute joints.

2.4.3. Summary

For the purpose of high speed manipulation of objects like crabs, robots with parallel mechanisms are required, which have the characteristics such as high velocity and acceleration, high loading capacity and high stiffness. In this regard, the authors focused on 3-RPR parallel robot with building rigid revolute joints.

2.5. Problem Statement

There are some functionality issues in different joints as mentioned in literature review including inadequate lubrication and high friction, having backlash, low rigidity and complex shapes and difficulty in assembly. One of the important kinds which is widely used is the revolute joint offering one rotational degree-of-freedom (DOF) between two rigid bodies. Moreover, the Cardan joint (universal joint) and ball joint featuring more DOFs with increased structure complexity are frequently used in many applications.

We wish to design rotational joints which include all of the desired factors such as self-centering and self-aligning, low friction, low backlash and high rigidity.

Therefore, there is a need to completely redesign these joints to fulfill the criteria.

2.6. Coordinate Measuring Machine

CMM is able to measure the workpiece to find the physical shape and dimension in Cartesian Coordinates. The data acquired from the machine are the coordinate position points of the workpiece whether just some points or parts or even the whole shape of workpiece. Therefore, this information can be used later by relevant software to make a comparison with the original CAD data or even create a 3D CAD if the source is not achievable [57][58].

CMM techniques are mainly used in rapid prototyping, reverse engineering, industrial design and quality control and inspection. It can be categorised as two major groups [59]:

1. Contact: includes measuring desired points of the object by using the contact probe of the CMM.
2. Noncontact: includes measuring the object through optical techniques including:
 - laser triangulation
 - Photogrammetric systems
 - measurement of beam returning time (TOF) systems
 - Structured light systems
 - Computed tomography (CT) systems
 - Magnetic resonance (MRI) systems

Each group has some advantages and disadvantages. In general, CMMs with contact method are suitable for higher accuracy and limited data points. In contrast, those machines with optic method are appropriate for lower accuracy with lots of data points (such as scanning a partial or whole workpiece surface) which are called cloud-points.



Figure 2-16 CMMs

A contact probe type from Mitutoyo Co.

An optical type from Nikon Metrology, Inc

2.7. Rapid Prototyping and Manufacturing

Rapid prototyping (RP) processes fabricate three dimensional (3-D) objects with complex shape directly from 3D-CAD models layer by layer. The main difference between traditional machining technology such as CNC and RP is the way of process. RP is the additive manufacturing (AM) process and CNC is the subtractive manufacturing (SM).

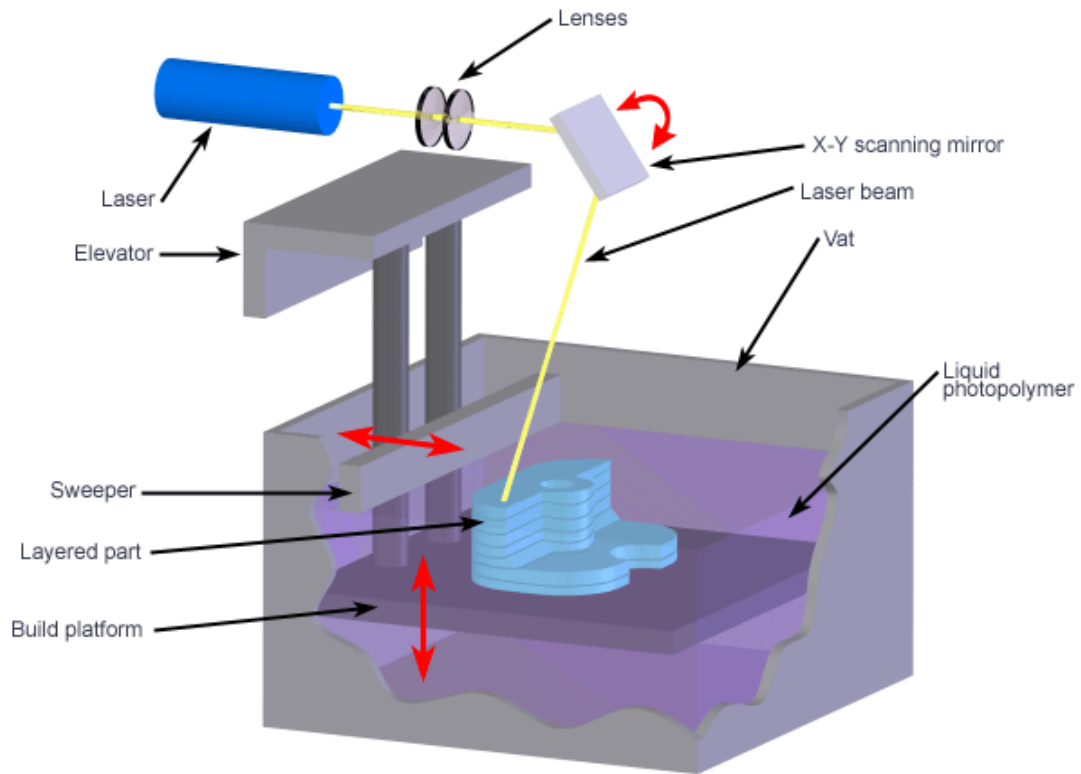
Speed, complexity of parts and the ability of producing the internal geometric as the same as external one are some of the advantages of RP over other technologies. AM technology can be used further than just prototyping including end products. Therefore, it can be called rapid prototyping and manufacturing [60].

The application of the RP process in automotive, aerospace, electrical industries, jewellery, medical, arts and architectural is well established [63]. Many RP systems are commercially available. Stereolithography (SL), selective laser sintering (SLS), binder jetting (BJ), and fused deposition modelling (FDM) are the most used systems in the market.

The brief introduction of each method along with the advantage and disadvantage are explained.

2.7.1. Stereolithography (SL)

Stereolithography uses an ultraviolet (UV) laser to solidify the liquid raw material which is photopolymer resin and can be solidified in exposed of UV. The 3D object is fabricated layer by layer based on the 3D CAD. The final part should be cleaned up from its support. The thickness of each layer is 0.06-0.15 mm [64].



Copyright © 2008 CustomPartNet

Figure 2-17 A schematic of stereolithography technology (has been provided Courtesy of CustomPartNet Inc) [65].

2.7.2. Binder Jetting

Another name of binder jetting is three-dimensional printing (3DP). The machine prints a binder and also inks (in those machine which are colorful) into a powder bed to fabricate a part. When one layer is printed, the powder bed goes down with the amount of a layer and a new layer of powder is distributed on that until the rest of the process. Typically, the binder diameter is 80 μm . A wide range of raw material such as polymer composite, metals, and ceramic materials are available [60].

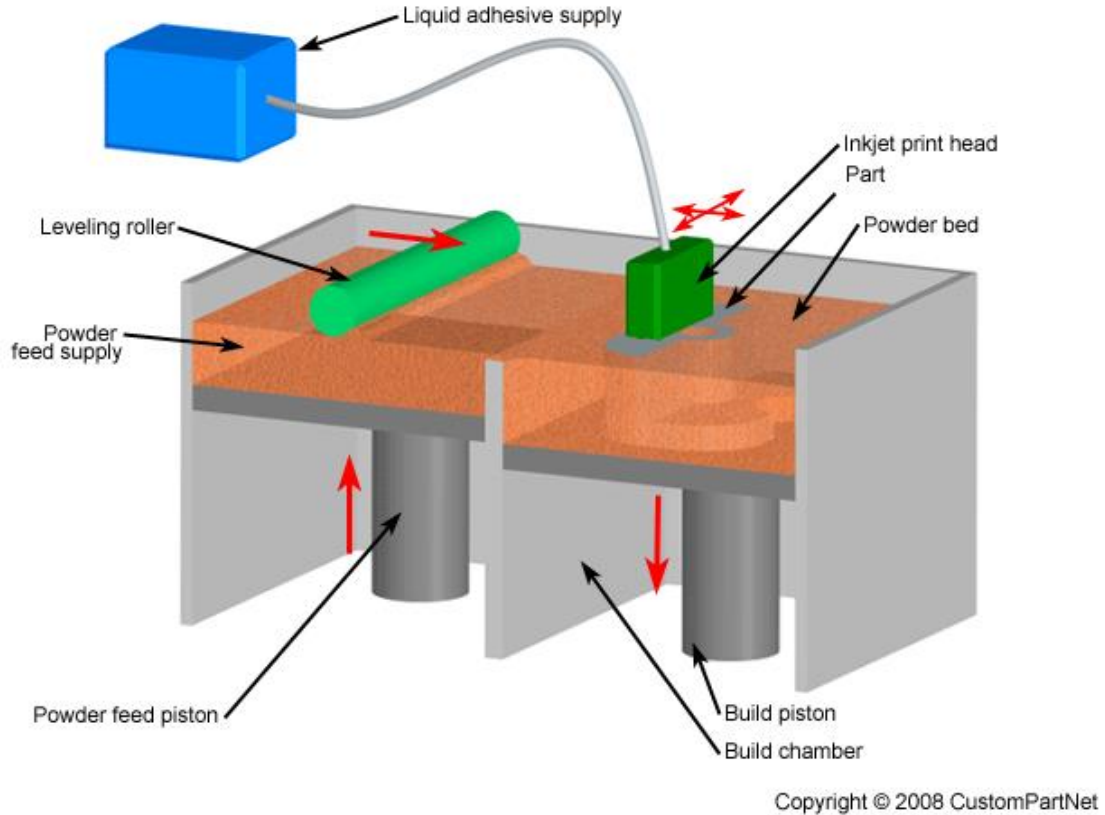
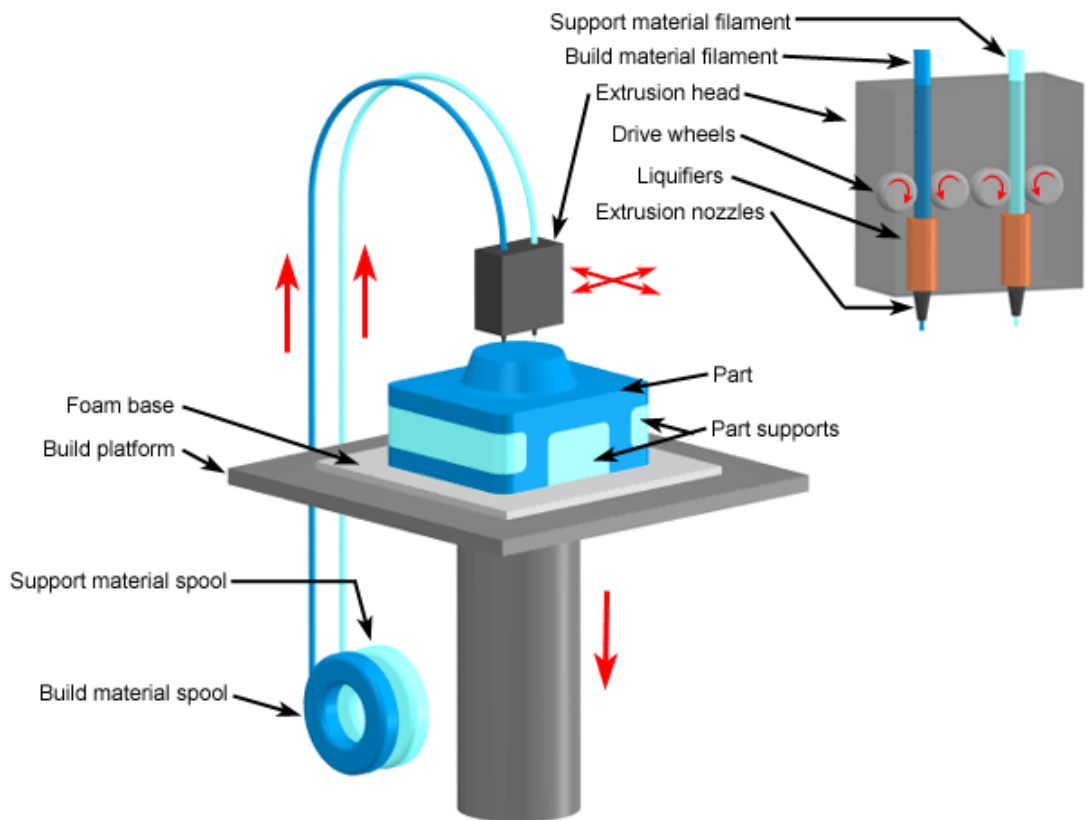


Figure 2-18 A schematic of binder jetting technology (has been provided Courtesy of CustomPartNet Inc) [61]

2.7.3. Fused Deposition Modeling (FDM)

In this technology, plastic materials in filament shape are used for the model and its support. The support material and build material go to extrusion nozzles and then the melted materials deposit in the current layer based on the tool-path from the CAD/CAM software. The extruded materials immediately harden and are glued to the new layer below it and all layers form with this pattern from bottom to top of the platform. At the end, the support material will be removed and cleaned up from the part. The raw materials are thermoplastic and the minimum layer thickness can be 0.076 mm so far [60].



Copyright © 2008 CustomPartNet

Figure 2-19 A schematic of fused deposition modeling technology (has been provided Courtesy of CustomPartNet Inc) [62]

2.7.4. Selective Laser Sintering (SLS)

SLS is one of the RP techniques, which uses powder material to create parts from CAD models layer by layer. High flexibility, no need to support material and superior mechanical properties are noticeable advantages of the process. The system uses an infrared laser beam to heat up a powder bed and to sinter the particles to a dense object according to the 3D CAD model. The thickness of each layer is 0.06-0.15 mm. Polymers, metals and ceramics powders are commonly used [66].

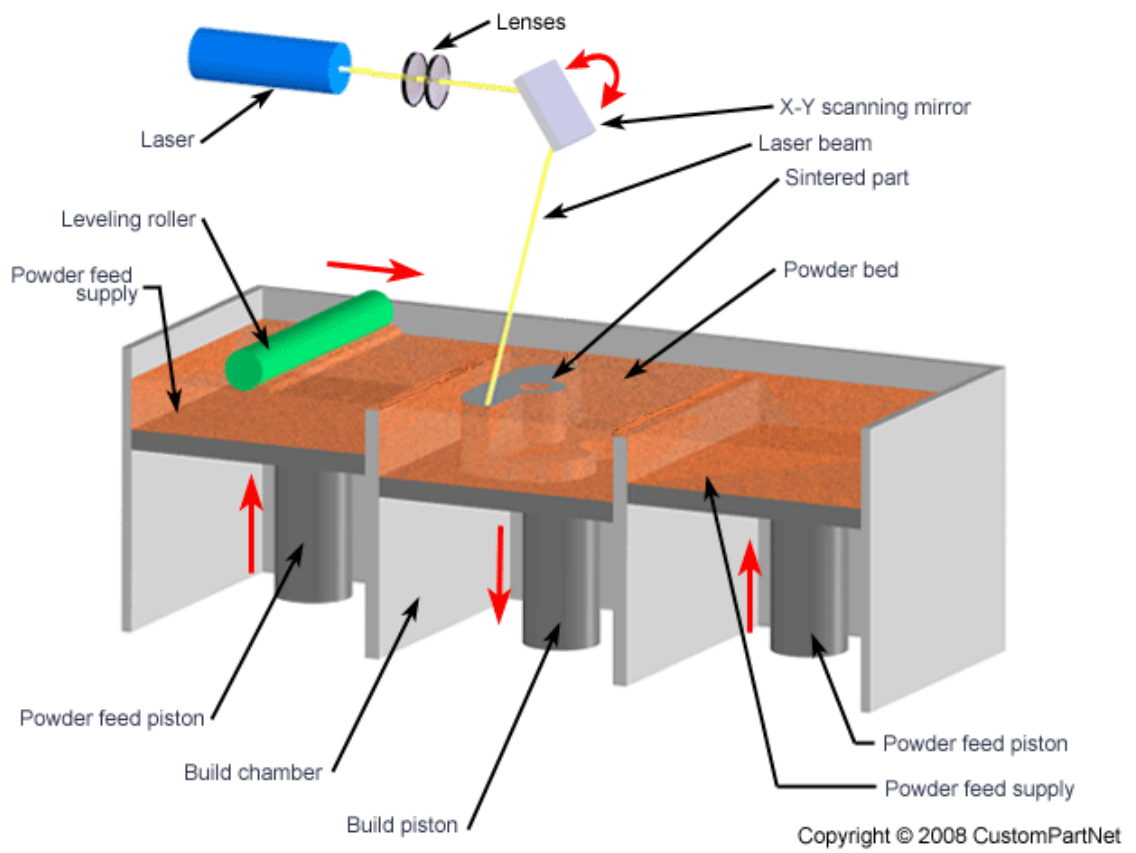


Figure 2-20 A schematic of Selective Laser Sintering technology (has been provided Courtesy of CustomPartNet Inc) [67]

2.7.5. The Comparison of RP Methods

Comparison chart between major rapid prototyping techniques [56]

Process	SLS	SLA	Binder Jetting	FDM
Description	Laser fusion in a powder bed	UV laser scanning vat polymerization	Particle binding in a powder bed	Extruded layers of thermoplastic
Details	Layers: 0.06-0.15 mm Features: 0.3mm Surface: rough Print speed: fast	Layers: 0.06-0.15 mm Features: 0.1mm Surface: smooth Print speed: average	Layers: 0.089-0.12 mm Features: 0.4mm Surface: rough Print speed: very fast	Layers: 0.076-0.3 mm Surface: very rough finish Print speed: slow
Pros	Strong Complex parts Large build volume Parts can be stacked in build volume Living hinges and snap features possible	Fine detail Smooth surface finish	Multicolor prints Fast print speed	High part strength Low cost
Cons	Grainy surface finish	Weak parts Susceptible to sunlight and heat	Very weak parts Rough surface finish	Poor surface finish Slow printing
Applications	Electronics housing Mounts Custom consumer products Aerospace hardware	Medical/dental products Electronics casings Investment casting patterns Art	Full color prototypes and objects Figurines	Electronics housing Mounts Custom consumer products

Chapter 3

Chapter 3: Design and 3D Print a Fully Articulated Crab

One of the works firstly carried out in this thesis was making a fully articulated snow crab.

The objectives of this work were:

- To create snow crab models with all details for robot manipulation testing as the real dead crabs would become a health and hygienic hazard.
- To design different rotational joints such as the revolute joint, ball joint and a combination of them in such a way that the motion of the real crab caused by its tendon is simulated by use of friction.
- To study the introduction of rigidity of the revolute joint families to improve the quality of the joints in the crab.
- This work would serve as excellent practice for the forthcoming rotational joint designs.

In this regard, a general description of the techniques and methods for CMM and 3D printing came in literature review to give an idea which one is more appropriate for our case. The 3D joint models are described in this chapter and finally their integration into a crab model is examined.

3.1. The Purpose of This Crab Joint Modeling

The team's work under Dr. Luc supervision at the High Performance Robotics Laboratory involves designing solutions for automated crab manipulation which would mostly be achieved utilizing high performance robots as it as explained in the former chapter.

In designing robots and grippers for crab manipulation, we have to test them and it cannot be done with the real crab for hygiene reasons so a crab physical model is needed. Because of the complexity shape of the real crab in terms of fabrication, the method of rapid prototyping was chosen. To proceed the fabrication, at first, scanning a crab with laser scanners should be done which was carried out by Stephen King and his team from the Marine Institute and the virtual model was provided. However, from a robotics manipulation point of view, their model was not realistic enough for being test applicable since they did not include articulated legs with appropriate joints.

This would then require a 3D model where joints are simulating the tendons. Therefore, designing a crab model was done to be as realistic as possible including tendons but those tendons cannot be modelled in a 3D printed one effectively. Real tendons, as they are found in crab joints, slow down the fall of legs when the crabs are manipulated. So, applying friction in joints as one of the solutions was executed which would render a similar slow leg fall.

Extensive research work should determine how to make the virtual model design for each type of leg joints as they are many different articulations in the crabs. It was tried to design joints identical to the real ones but design some which provide similar behaviors.

A compromise between exactness and design simplicity in the context of rapid prototyping should be chosen.

3.2. The Joint Models for the Snow Crab

The 3D model of a rigid snow crab was scanned and digitized by the Seafood Processing team at Marine Institute of Memorial University of Newfoundland. Figure 3-1 shows the 3D model before modifying it.

The joint type in the claw leg attached to the body of a real snow crab is the ball joint with motion ranges limited by tendons. The secondary limbs are connected through a type of revolute joint which is also limited in displacement by tendons.

To reach the full motion range of the claw leg, the primary ball joint is modeled by a ball joint and a revolute joint and they were adapted to a snow crab model. Three joints were designed.



Figure 3-1 A schematic of a real snow crab [68]

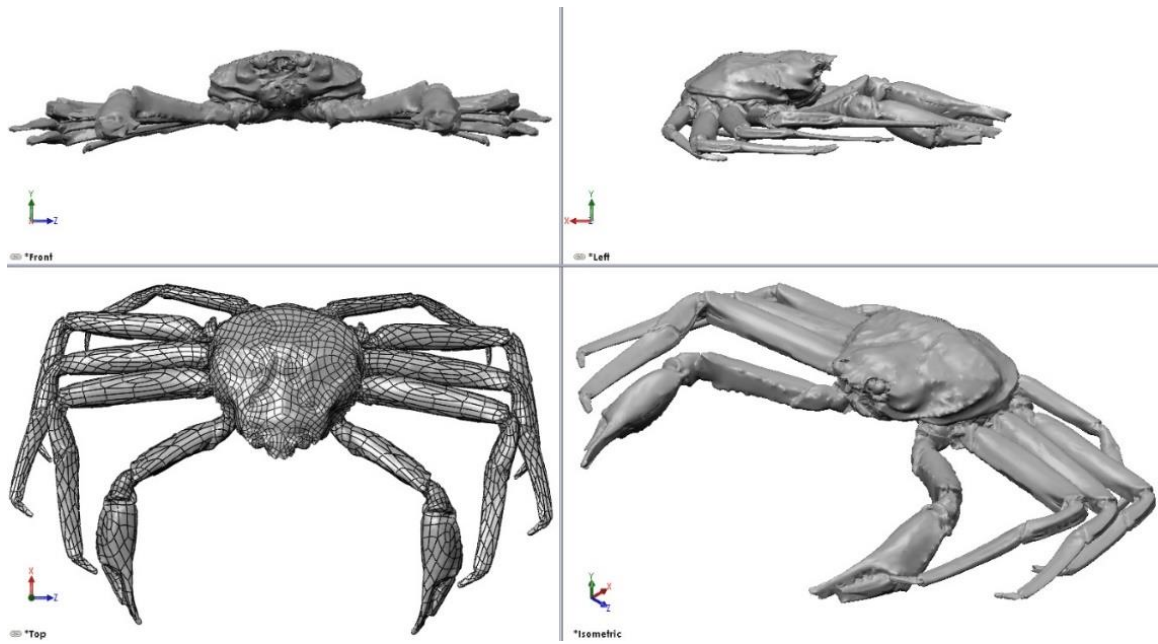


Figure 3-2 The 3D scan model of a snow crab (courtesy of the Marine Institute)

3.2.1. Fork Ball Joint Used in the Back Legs

The real snow crab uses ball joint attaching the back legs to the body and gives it three degrees of freedom. Using a common ball joint is not functional since there is limited space between each legs joint with large range of motion. Therefore, a specific kind of ball joint was designed and named Fork Ball Joint (Figure 3-3).

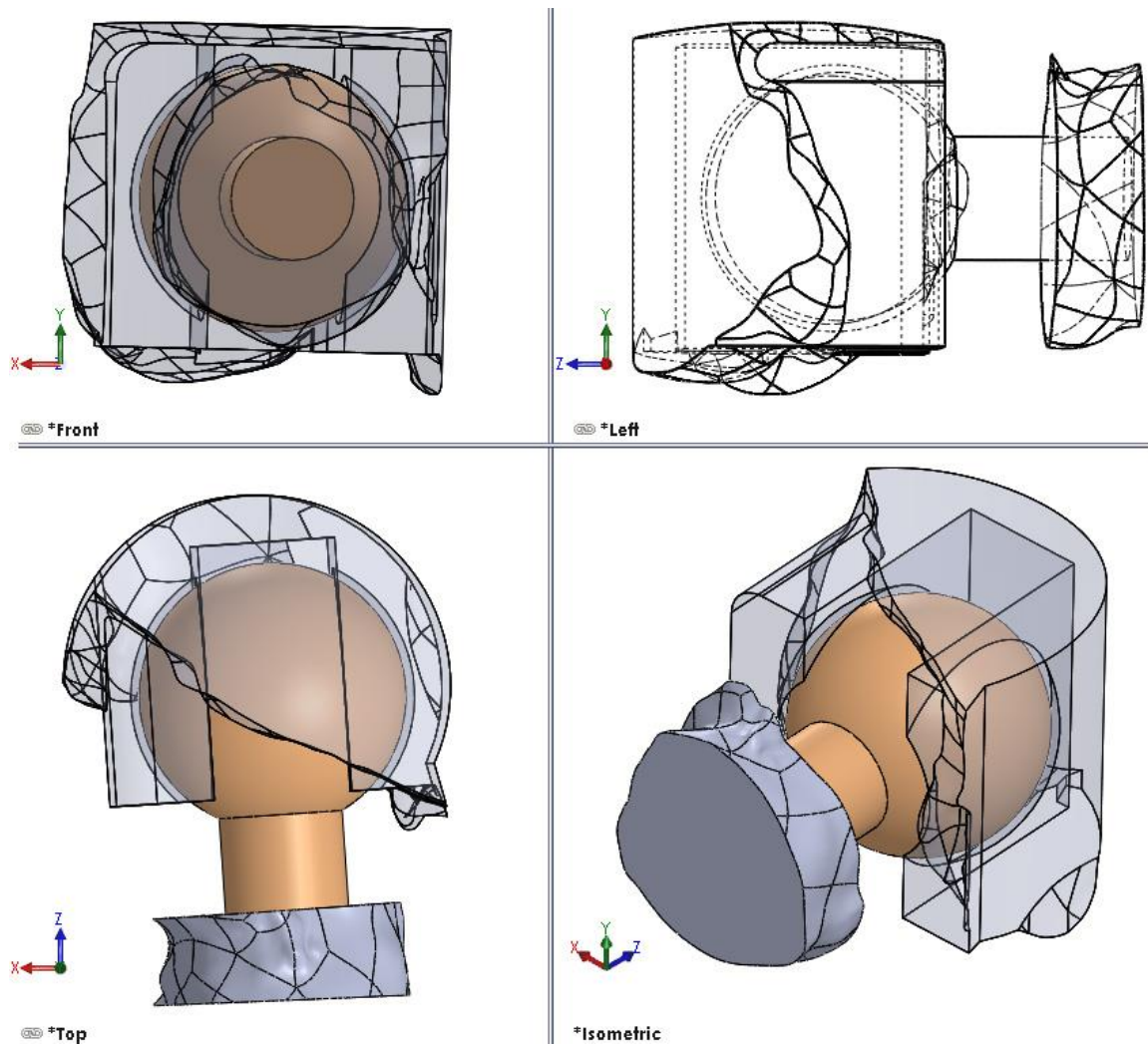


Figure 3-3 The fork ball joint used in each back leg

3.2.2. Revolute Joint for All the Knee Legs

The joint type used in the real crab knees is similar to any revolute joint. In this regard, a typical revolute joint was designed. In order to simulate the real one, the range of movement was limited to 180 degrees (Figure 3-4).

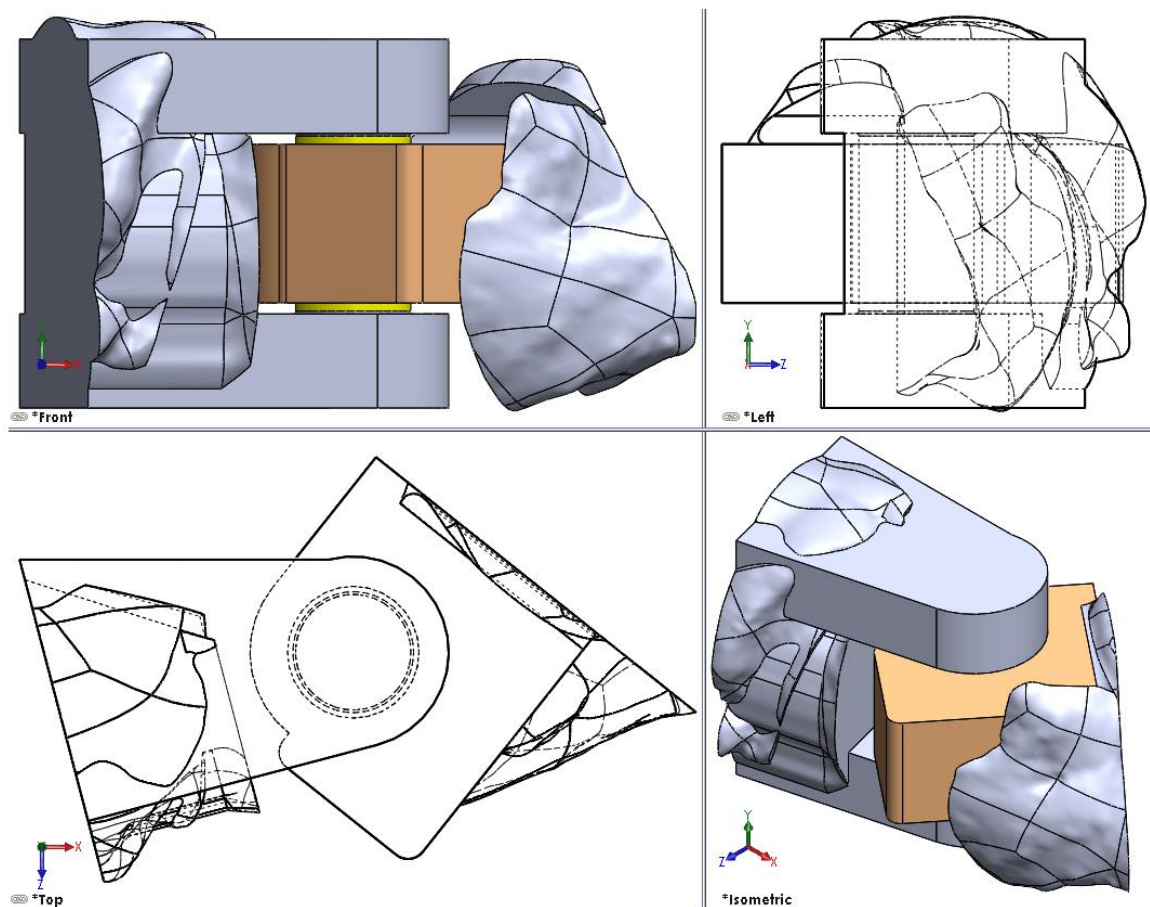


Figure 3-4 The sketch of revolute joint for the knees

3.2.3. Combination of Revolute and Ball Joint Used in the Claw Leg

One of the challenging design problems was the ball joint used in the claw leg to attach it to the body in a real snow crab. The tendon elasticity ability of the ball joint causes the high range of movement, meaning the extension of the claw leg particularly towards the front. After several designs, the combination of the revolute joint and ball joint was selected. They were designed very close to each other (Figure 3-5).

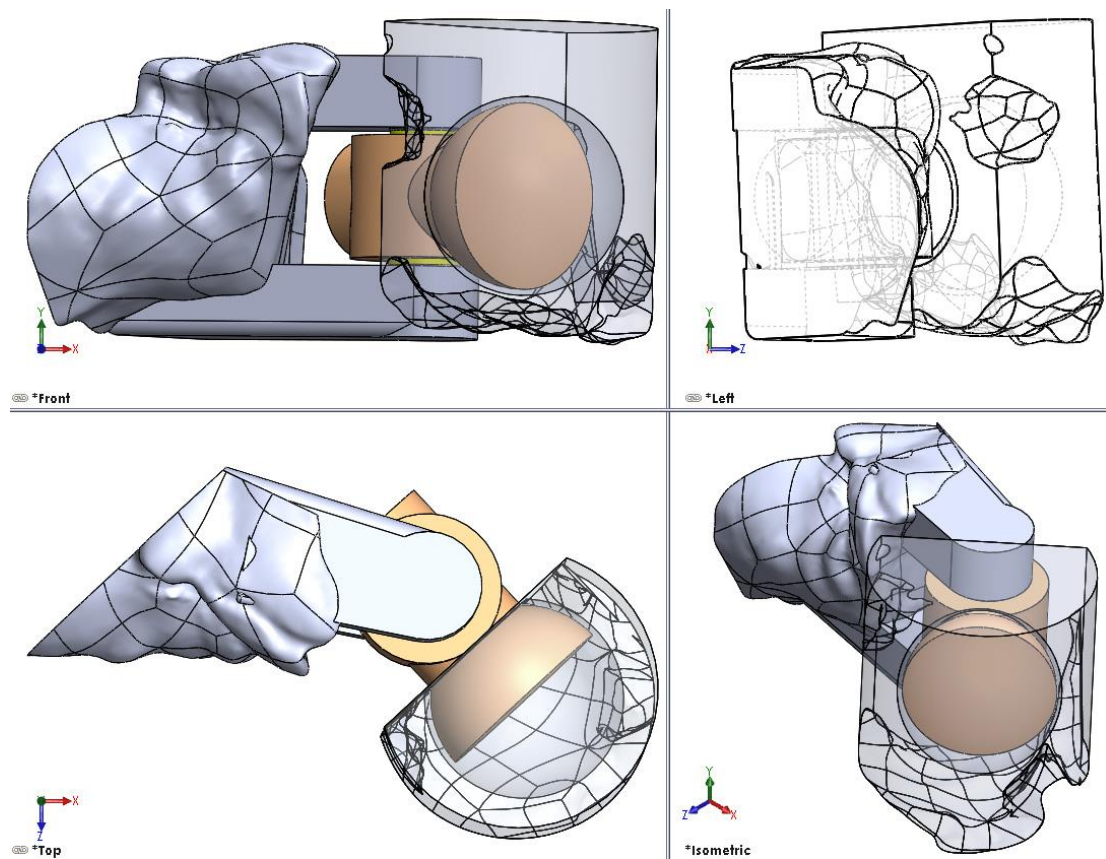


Figure 3-5 The combination of revolute joint and ball joint used in the claw leg

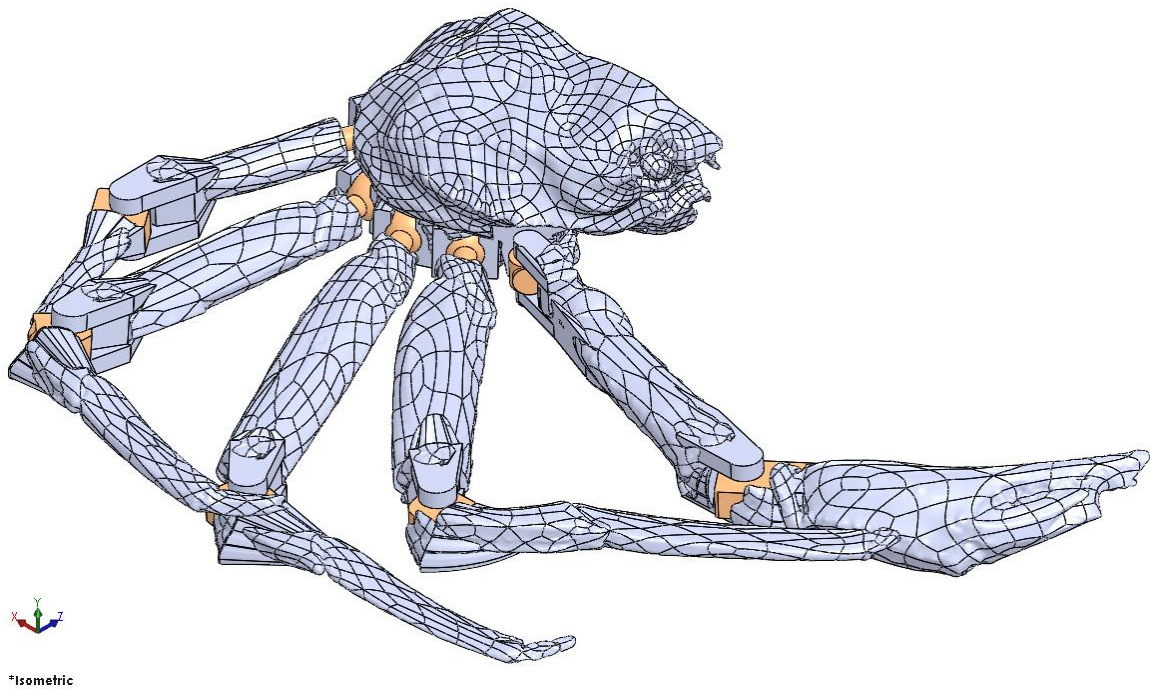


Figure 3-6 The fully articulated snow crab model

3.3. Prototyping the Snow Crab

After designing a fully articulated crab, a half crab was cut from the complete model (Figure 3-6). The reason was that the crab process under study involved half crabs coming out of a standard butchering machine.

3.3.1. Manipulation of the 3D Model in the CAD Program

The 3D model that was used and given to us by the Marine Institute was in SOLIDWORKS format (SLDPRT and SLDASM). The designing of different joints was done on the 3D model as described in previous sections to accomplish the fully articulated crab.

Afterwards, each test model and eventually the final model were sent to RP machines with STL format, common 3D Printers format.

3.3.2. Producing the 3D Physical Model

FDM and SLS (Figure 3-7) were selected to prototype the crab since the FDM parts has acceptable surface finish as well as strength and SLS parts are very strong.

The half snow crab model was produced in the FDM machine at 0.7 scale and SLS at 1.0 scale.

The joint interface clearance was carefully selected after producing some small test parts in each FDM and SLS to find out the minimum possible gap at the pair interface specifying the part tolerances (Figure 3-8). Several trials with various tolerances including the clearances of 0.2, 0.25, 0.3, 0.35, 0.4 and 0.5 mm were done as the joint should feature friction mimicking the effect of the leg tendons.



Figure 3-7 RP machines at Memorial University

FDM - Fortus 400mc from Stratasys Ltd.

SLS – sPro from 3D Systems Corporation



Figure 3-8 Different trials with various tolerances

The minimum clearance of 0.3 mm (not loose and not too tight) coincidentally worked in both machines whereas the movement of the joints was smooth and simulated a real crab movement.

The crab produced by FDM had better surface finishing and the one by SLS was much stronger. Therefore, depending on the type of the applications, each model can be used. The following figures show the results.



Figure 3-9 The fully articulated snow crab produced by FDM (the scale factor 0.7:1)



Figure 3-10 *The fully articulated snow crab produced by SLS*



Figure 3-11 *The fully articulated snow crab produced by SLS (the scale factor 1:1)*

Chapter 4

Chapter 4: Joint Design

4.1. Revolute Joint

The principal goal of this research is to design a revolute joint which can meet the following criteria:

- a) Maximizing rigidity
- b) Self-centering and self-aligning
- c) Minimizing backlash
- d) Minimizing friction

In order to achieve the mentioned points, a revolute joint in a conical shape was chosen and eventually referred to as a conical joint alone in current work (Figure 4-1). As it was mentioned in section 1.1., one of the inspiring reasons to choose a conical shape was the prismatic joints in machine-tools. Moreover, we can make circular and obtain the same advantages.

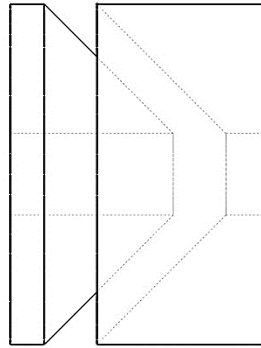


Figure 4-1 A schematic of a revolute joint in conical shape

The two parts of the joints can be fixed together by nut, bolt, nut and spring, or even cam and forelock. Nut and spring mechanism were chosen because of the adjusting flexibility of the spring force.

However, the contact surfaces of inner and outer joint can play a key role in order to minimize the friction. There are some options to fill the gap of joint parts:

- 1- Using oil or grease as a lubricant between the contact surfaces
- 2- Using solid film or dry friction as a lubricant between the contact surfaces
- 3- Using a sleeve between the joint parts
- 4- Using two sleeves between the joint parts

4.2. Dry Friction

Since friction is one the important key roles in the optimization of the revolute joint, the definition of friction is given in this section to give an idea for following up.

Friction is a force that resists relative tangential or intended motion with the opposite direction. Dry friction or Coulomb friction happens between two solid bodies. Dry friction can cause elastic or plastic deformations and it interacts with the surface of contact areas where wear can result [83].

The laws of dry friction rely more on experimental evidences. Their approximations are sufficiently adequate for many engineering applications and these will require verification through experiments then. Some of the laws are as follows [82],[83]:

- The frictional force is directly proportional to the normal force between the contact area.
- The frictional force direction is opposite to the movement.
- The frictional force depends on the nature of the surfaces and materials. The rougher the surface, the higher the friction force.
- The frictional force is independent of the particular pressure between contact areas.
- The frictional force is independent of the velocities of the sliding parts.

4.3. Conical Joint Optimization

One of the most significant parameters in the design of the conical joint is its taper angle (the Conical Taper is defined as “the change in the diameter of a circular solid along its length” [84]). It affects the friction and finally the transmitted torque, the torque which is transferred from one part of the joint to the other part. Therefore, the design should fulfill two purposes, minimum and constant friction coefficients [85]. The constant friction is less

important in our case since there is a small length (the circumference circle of cross sectional joint) in the conical joint compared to the length of linear motion joint like what is used in Cartesian Robots, which is much longer than the length of circumference. Hence, it is aimed to reach the minimum friction as an effective role in the design of the conical joint.

In order to minimize the friction, we can proceed with either static or dynamic analysis. On the other hand, due to the fact that the static friction coefficient is usually larger than the dynamic one based on Coulomb's Law [86], the static analyses were performed, being a conservative evaluation. In this regard, if the amount of static friction could be minimum, it would definitely have a lower amount in dynamic motion, leading to a moving joint sustaining a lesser amount of friction while in rotational motion. Thus, it meets our criteria.

In some conditions such as motion in the air, the dynamic friction (drag force) may be larger than static friction but this only occurs if the relative motion of the joint is extremely fast and the shape of the object is large (such as the motion of the air plane in the sky). However, this study doesn't consider with air resistance.

There are 4 conditions which are analysed:

- Simple planar case in both vertical and horizontal directions
- 3D model in both vertical and horizontal directions

Some features of the joint are carefully considered including:

- i. The coordinate system of the joint is based on the Denavit and Hartenberg (D–H) convention.
- ii. The equivalent masses of each joint parts, lead to equivalent results in one direction.
- iii. Designing the main joint without the sleeves and adding them afterwards.

4.3.1. Optimization of Simple Planar Case in Vertical Direction

If there is any tendency for joint motion of the two interface parts along axial direction (Z axis), the goal is to reduce the friction in order for joint parts to fit easier and faster into their stable position.

In this case, the direction of gravity is alongside the main axis (Z axis) of the conical joint (Figure 4-2). The motion is studied as a result of spring force without any actuator torque in this step.

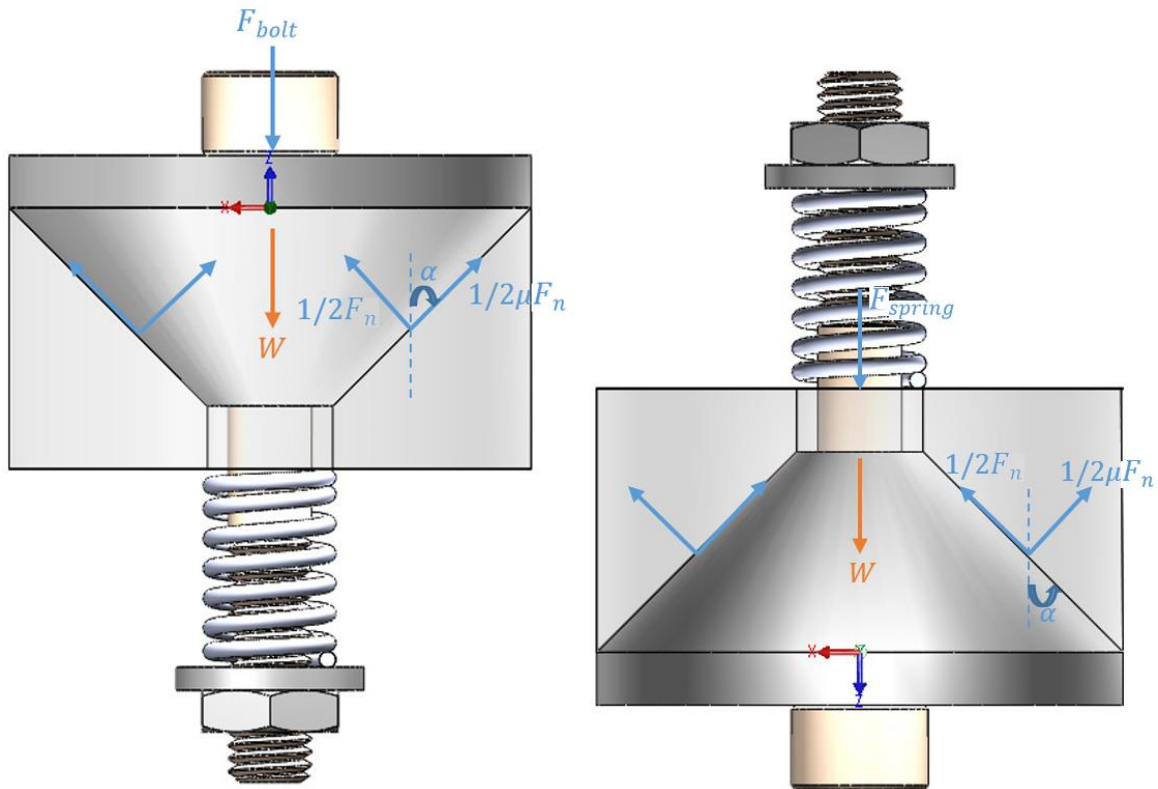


Figure 4-2 The case in which the direction of gravity is alongside the main axis (Z axis)

a) FBD of inner joint

b) FBD of outer joint

The following equations are known:

$$F_{spring} = F_{bolt} \quad (4.1)$$

$$m_{inner\ joint} = m_{outer\ joint} = m \quad (4.2)$$

$$f = \mu_s F_n \quad (4.3)$$

where f is static friction, μ_s is the static coefficient, F_n is the normal force, $m_{inner\ joint}$ is the mass of inner joint, $m_{outer\ joint}$ is the mass of outer joint and both are equal, F_{spring} is the force applied from spring and F_{bolt} is the force applied from bolt.

a) FBD of inner joint

Consider the case in Figure 4-2-a

$$\sum F_y = 0 \quad (4.4)$$

$$mg + F_{bolt} - f \cos \alpha - F_n \cos \left(\frac{\pi}{2} - \alpha \right) = 0 \quad (4.5)$$

$$F_n [\mu_s \cos \alpha + \sin \alpha] = mg + F_{bolt} \quad (4.6)$$

In order to minimize the friction, F_n should be minimized and in order to minimize F_n , its coefficient $[\mu_s \cos \alpha + \sin \alpha]$ should be maximized.

μ_s for Carbon Steel: 0.14

$\alpha = 82^\circ$ when $[\mu_s \cos \alpha + \sin \alpha]$ is maximized.

b) FBD of outer joint

Consider Figure 4-2-b:

$$\sum F_y = 0 \quad (4.7)$$

$$mg + F_{spring} - \mu_s F_n \cos \alpha - F_n \cos \left(\frac{\pi}{2} - \alpha \right) = 0 \quad (4.8)$$

$$F_n [\mu_s \cos \alpha + \sin \alpha] = mg + F_{spring} \quad (4.9)$$

The equation 4.9 is the same formula and the same result as equation 4.6 in case a) since both inner joint and outer joint have the same mass and corresponding geometric shape.

4.3.2. Optimization of Simple Planar Case in the Horizontal Direction

There is the same goal in the vertical direction as in the previous section but with a different joint orientation.

In this case, the direction of gravity is perpendicular to the main axis (Z axis) of the conical joint (Figure 4-3). The motion is studied as a result of the spring force without any actuator torque in this step.

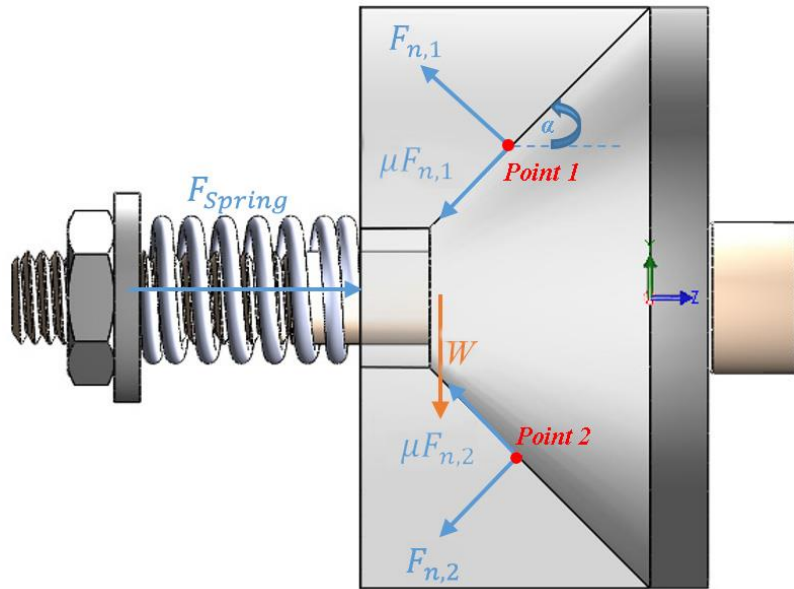


Figure 4-3 The direction of gravity is perpendicular to the main axis (Z axis) - FBD of outer joint

$$\sum F_y = 0 \quad (4.10)$$

$$\begin{aligned} -W + F_{n,1} \cos \alpha - F_{n,2} \cos \alpha \\ - \mu_s F_{n,1} \sin \alpha + \mu_s F_{n,2} \sin \alpha = 0 \end{aligned} \quad (4.11)$$

$$\cos \alpha (F_{n,1} - F_{n,2}) + \sin \alpha (-\mu_s F_{n,1} + \mu_s F_{n,2}) = W \quad (4.12)$$

$$\begin{aligned} -\cos \alpha (-F_{n,1} + F_{n,2}) + \mu_s \sin \alpha (-F_{n,1} + F_{n,2}) \\ = W \end{aligned} \quad (4.13)$$

$$(F_{n,2} - F_{n,1})(\mu_s \sin \alpha - \cos \alpha) = W \quad (4.14)$$

$$F_{n,2} - F_{n,1} = \frac{W}{\mu_s \sin \alpha - \cos \alpha} = a \quad (4.15)$$

$$\sum F_x = 0 \quad (4.16)$$

$$\begin{aligned} F_{spring} - \mu_s F_{n,1} \cos \alpha - \mu_s F_{n,2} \cos \alpha \\ - F_{n,1} \sin \alpha - F_{n,2} \sin \alpha = 0 \end{aligned} \quad (4.17)$$

$$F_{spring} = \mu_s \cos \alpha (F_{n,1} + F_{n,2}) + \sin \alpha (F_{n,1} + F_{n,2}) \quad (4.18)$$

$$F_{spring} = (\mu_s \cos \alpha + \sin \alpha)(F_{n,1} + F_{n,2}) \quad (4.19)$$

$$F_{n,1} + F_{n,2} = \frac{F_{spring}}{\mu_s \cos \alpha + \sin \alpha} = b \quad (4.20)$$

$$a, b \Rightarrow F_{n,2} = \frac{a + b}{2}, F_{n,1} = \frac{b - a}{2} \quad (4.21)$$

$$F_{n,1} = 1/2 \left[\frac{F_{spring}}{\mu_s \cos \alpha + \sin \alpha} - \frac{W}{\mu_s \sin \alpha - \cos \alpha} \right] \quad (4.22)$$

$$F_{n,2} = 1/2 \left[\frac{W}{\mu_s \sin \alpha - \cos \alpha} + \frac{F_{spring}}{\mu_s \cos \alpha + \sin \alpha} \right] \quad (4.23)$$

where W is the weight of outer joint, $F_{n,1}$ is the normal force to the outer joint from the highest point and $F_{n,2}$ is the normal force to the outer joint from the lowest point.

There is an important point here in that the amount of $F_{n,1}$ is the maximum and $F_{n,2}$ is the minimum throughout the contact area among all normal forces at each point. When the weight of the system is considered, the pressure in point 1 is the maximum and the pressure in point 2 is the minimum. In addition, the amount of $F_{n,1}$ is higher than F_n from the case of vertical direction in the previous section. It results in higher pressure in some areas and therefore has the potential to lead to a higher rate of wear and finally, a lower life time of the joint in the horizontal direction compared to the vertical direction.

In order to minimize the friction, $F_{n,1}$ should be minimized. Since W and μ_s are constant, so the value of $F_{n,1}$ depends on F_{spring} .

- a) Let's say each F_{spring} and W are $20N$ (see Figure 4-4)
- b) Let's say $F_{spring} = 200N$ and $W = 20N$ (see Figure 4-5)

Input interpretation

minimize	$0.5 \left(\frac{20}{\sin(\alpha) + 0.14 \cos(\alpha)} - \frac{20}{0.14 \sin(\alpha) - \cos(\alpha)} \right)$
----------	--

Local minima

$$\min \left\{ 0.5 \left(\frac{20}{\sin(\alpha) + 0.14 \cos(\alpha)} - \frac{20}{0.14 \sin(\alpha) - \cos(\alpha)} \right) \right\} \approx \frac{28.0111 \cos(6.28319 n)}{\cos^2(6.28319 n) - \sin^2(6.28319 n)} \text{ at } \alpha \approx 0.646302 + 6.28319 n \text{ for integer } n$$

Plot

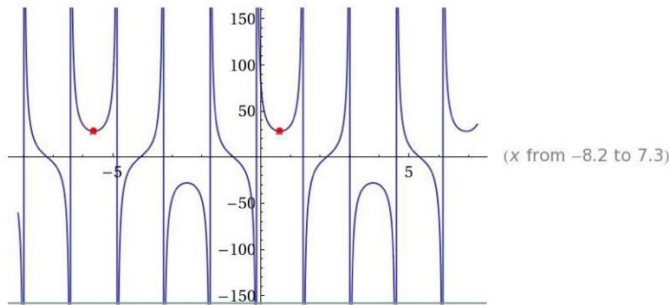


Figure 4-4 Min $F_{n,1}$ at $\alpha = 0.64$ rad or 37°

Input interpretation

minimize	$0.5 \left(\frac{200}{\sin(\alpha) + 0.14 \cos(\alpha)} - \frac{20}{0.14 \sin(\alpha) - \cos(\alpha)} \right)$
----------	---

Local minima

$$\min \left\{ 0.5 \left(\frac{200}{\sin(\alpha) + 0.14 \cos(\alpha)} - \frac{20}{0.14 \sin(\alpha) - \cos(\alpha)} \right) \right\} \approx \frac{714.286}{7.14286 \sin(6.28319 n + 0.997135) + \cos(6.28319 n + 0.997135) + 10.} + \frac{\cos(6.28319 n + 0.997135) - 0.14 \sin(6.28319 n + 0.997135)}{10.} \text{ at } \alpha \approx 0.997135 + 6.28319 n \text{ for integer } n$$

Plot

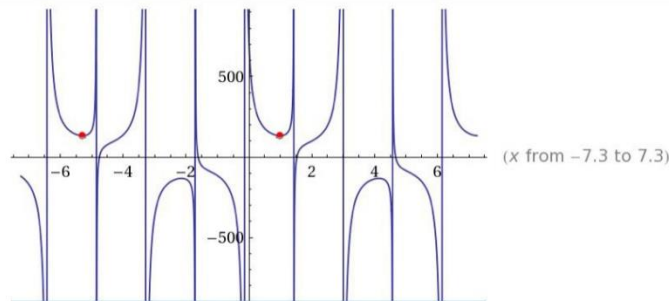


Figure 4-5 Min $F_{n,1}$ at $\alpha = 0.99$ rad or 57°

Figure 4-6 shows the trend ratio of F_{spring}/W with $W =$ constant, F_{spring} is variable) in terms of α . Increasing the above ratio leads to approach the α angle to higher amount (1.5 Radian or 85°) when minimum friction is desired.

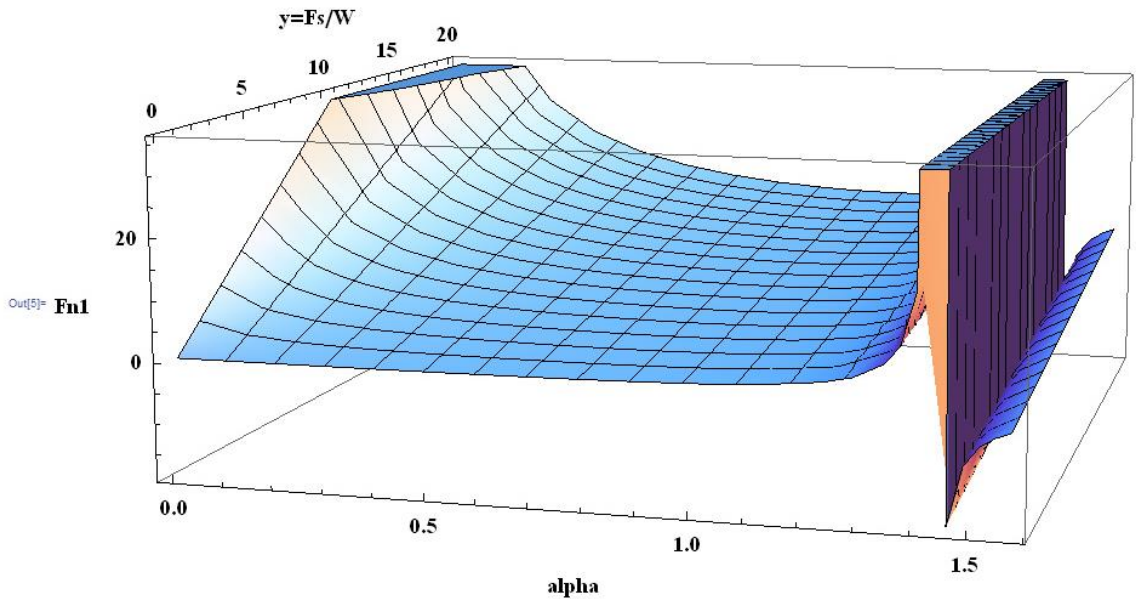


Figure 4-6 Trend ratio of F_{spring}/W

$W = \text{constant}, F_{spring}$ is variable in terms of variation of α .

Now we turn to next question which is: Do we need to design the conical joint for both axes at the same time?

Because the optimum angle in each axis can be different, we can have a better result if we focus on one axis and consider the criteria in accordance with that single axis.

At the end, it should be mentioned that the direction of friction force in the last two sections is valid until there is no torque along the axial axis and the joint parts are going to

set and sit with each other. An example of separating the parts and returning to the stable position is inertial forces along the axial axis (Z axis). As soon as every part is in place in the stable position, the amount of friction in that direction doesn't affect the transmitted torque. In order to find the minimum transmitted torque, we have to study the case in a three dimension which is coming in the next sections.

4.3.3. Optimization of 3D Model Case in Vertical Direction

When the conical joint in three dimension (3D) is considered, all the boundaries, which were already considered in two dimension (2D), convert to surfaces. As a consequence, the joint, in reality, deals with distributed pressure and friction. Therefore, in order to find more accurate results, the 3D Model Case was studied. Figure 4-7 shows the location in absolute coordinates.

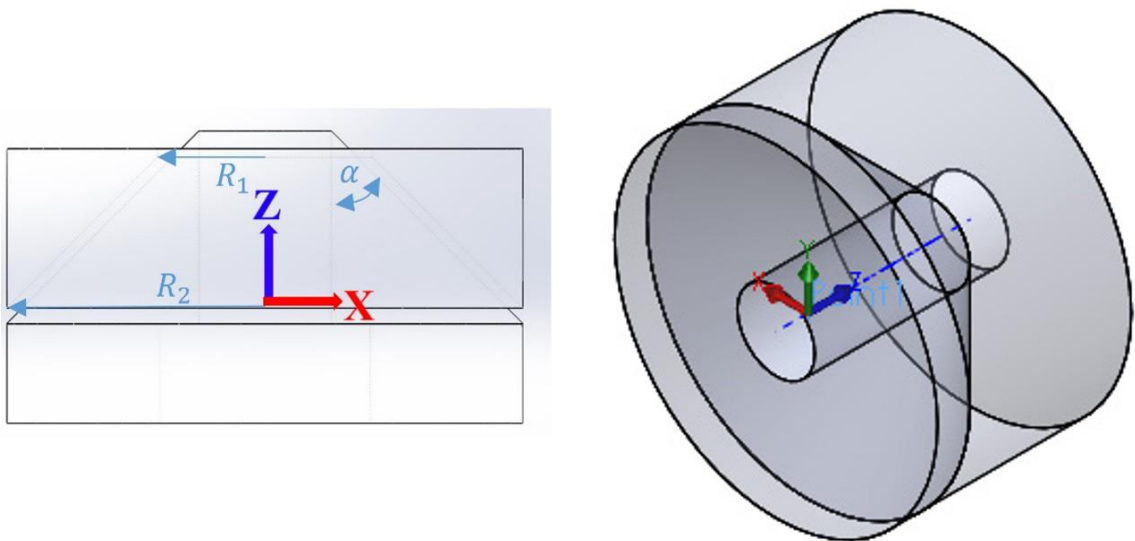


Figure 4-7 The revolute conical joint and the location of reference frame

The next step was to find a suitable taper angle in terms of minimum friction caused by the mechanism geometry and overcoming the reaction forces impacts.

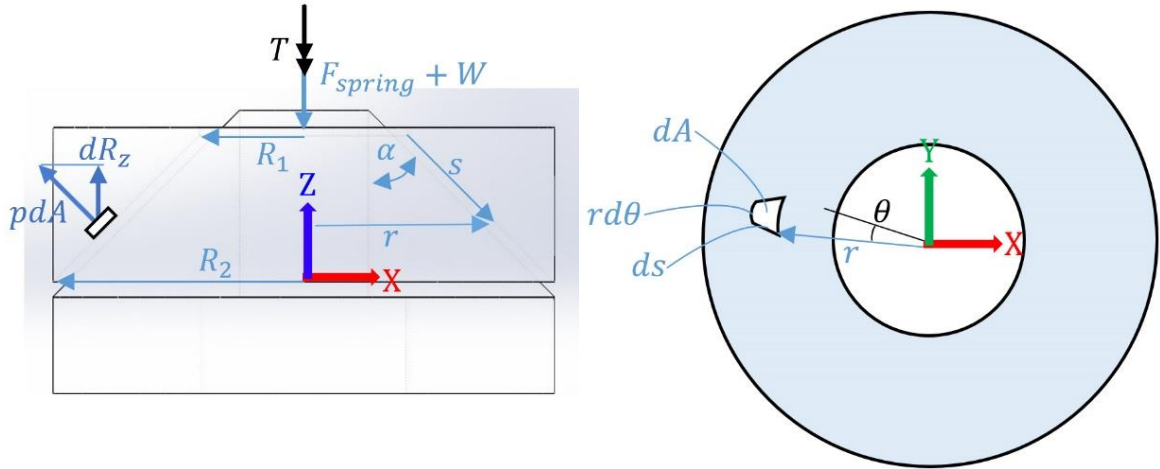


Figure 4-8 The free body diagram for outer joint

The minimum friction leads the minimum transmitted frictional torque T is determined by equation 4.24 and 4.25 [79].

Uniform pressure assumption is:

$$T = \frac{2}{3} \frac{\mu_s (F_{spring} + W)}{\sin \alpha} \left[\frac{R_2^3 - R_1^3}{R_2^2 - R_1^2} \right] \quad (4.24)$$

Uniform wear assumption is:

$$T = \frac{1}{2} \frac{\mu_s (F_{spring} + W)}{\sin \alpha} (R_2 + R_1) \quad (4.25)$$

where μ_s is the coefficient of static friction, F_{spring} is the force of the spring, W is the weight of the upper joint parts, α is the taper angle, and R_1 and R_2 are the radiuses of the conical joint (Figure 4-8). In addition, the complete calculations are given as follows.

A new bearing joint can distribute the pressure evenly over the rubbing surfaces which leads to proper contact between the shaft and joint over the whole surface. However, due to surface friction, the joint will wear out after a while and consequently the relative motion at the surface in different parts of bearing will no longer be the same. Moreover, the wear will be different at various radiuses causing non-uniformity in the pressure distribution. It is worth noting that the pressure and the rubbing velocities between the surfaces determine the rate of wear of surfaces.

The design of the joint is based on the following assumptions:

Case A: that uniform pressure is distributed throughout the contact surfaces

Case B: that there is uniform wear throughout the contact surfaces [79], [80], [81].

The full calculations to find transmitted frictional torque T (refer to the diagram of Figure 4-8) are given below:

$$\sum F_z = 0 \quad (4.26)$$

$$-W - F_{spring} + R_z = 0 \quad (4.27)$$

where R_z is the Z force component resulting from the pressure p .

$$dA = rd\theta \times ds \quad (4.28)$$

$$r/s = \sin \alpha \quad (4.29)$$

$$ds = dr / \sin \alpha \quad (4.30)$$

From Eq. (4.28) we conclude:

$$dA = rd\theta \times dr / \sin \alpha \quad (4.31)$$

The normal force on dA generates the pressure p on dA is defined as:

$$dN = pdA = prd\theta dr / \sin \alpha \quad (4.32)$$

Vertical load transmitted on dA is determined by:

$$dR_Z = pdA \sin \alpha = prd\theta dr \quad (4.33)$$

The total transmitted vertical load is:

$$R_Z = \int_A dR_Z = \int_A prd\theta dr \quad (4.34)$$

Case A: Uniform Pressure

$$R_Z = \int_A prd\theta dr = p \int_{R_1}^{R_2} r \int_0^{2\pi} d\theta dr \quad (4.35)$$

$$R_Z = \pi p (R_2^2 - R_1^2) \quad (4.36)$$

On the other hand from Eq. (4.27) we can obtain:

$$p = \frac{(F_{spring} + W)}{\pi(R_2^2 - R_1^2)} \quad (4.37)$$

The frictional force on the element dA is:

$$df = \mu_s \times \left(\frac{pr d\theta dr}{\sin \alpha} \right) \quad (4.38)$$

The torque produced by the friction force is determined by:

$$dT = \mu_s \times \left(\frac{pr d\theta dr}{\sin \alpha} \right) \times r \quad (4.39)$$

The total transmitted frictional torque is:

$$T = \int_{R_1}^{R_2} \int_0^{2\pi} \mu_s \left(\frac{pr^2 d\theta dr}{\sin \alpha} \right) = \frac{\mu_s p}{\sin \alpha} \int_{R_1}^{R_2} r^2 \int_0^{2\pi} d\theta dr \quad (4.40)$$

If p is substituted with Eq. (4.37), we have:

$$T = 2/3 \frac{\mu_s (F_{spring} + W)}{\sin \alpha} \left[\frac{R_2^3 - R_1^3}{R_2^2 - R_1^2} \right] \quad (4.41)$$

Case B: Uniform Wear

We know that:

$$p \times r = \text{Constant (say } C) \quad (4.42)$$

$$p = C/r$$

The total transmitted vertical load from Eq. (4.34) becomes:

$$\begin{aligned} R_Z &= \int_A prd\theta dr = \int_{R_1}^{R_2} \int_0^{2\pi} Cd\theta dr & (4.43) \\ &= C \int_{R_1}^{R_2} \int_0^{2\pi} d\theta dr = 2\pi C(R_2 - R_1) \end{aligned}$$

On the other hand from Eq. (4.27), we have:

$$R_Z = F_{spring} + W = 2\pi C(R_2 - R_1) \quad (4.44)$$

$$C = \frac{F_{spring} + W}{2\pi(R_2 - R_1)} \quad (4.45)$$

The total transmitted frictional torque from Eq. (4.39) is calculated as:

$$\begin{aligned} T &= \int_{R_1}^{R_2} \int_0^{2\pi} \mu_s \left(\frac{pr^2 d\theta dr}{\sin \alpha} \right) = \frac{\mu_s C}{\sin \alpha} \int_{R_1}^{R_2} r \int_0^{2\pi} d\theta dr & (4.46) \\ &= \frac{\pi \mu_s C (R_2^2 - R_1^2)}{\sin \alpha} \end{aligned}$$

If C is substituted from Eq. (4.45), we have:

$$T = 1/2 \frac{\mu_s (F_{spring} + W)}{\sin \alpha} (R_2 + R_1) \quad (4.47)$$

The design consideration with regards to one of the assumptions should be looked at in order to have safe and conservative results. In our case, designing a joint which achieves the minimum friction and thereby minimum torque is desired and dealing with a formula that causes higher torque (so uniform pressure assumption is selected) leads us to the optimum joint that satisfies the Eq. (4.24).

Considering the behavior of $\sin \alpha$ in the denominator, if other variables are fixed, the minimum frictional torque transmitted is achieved when α approaches 90 degrees.

A graphic comparison with friction torques and axial loads with assumptions of uniform pressure and uniform wear has been reproduced from [82] (Figure 4-9).

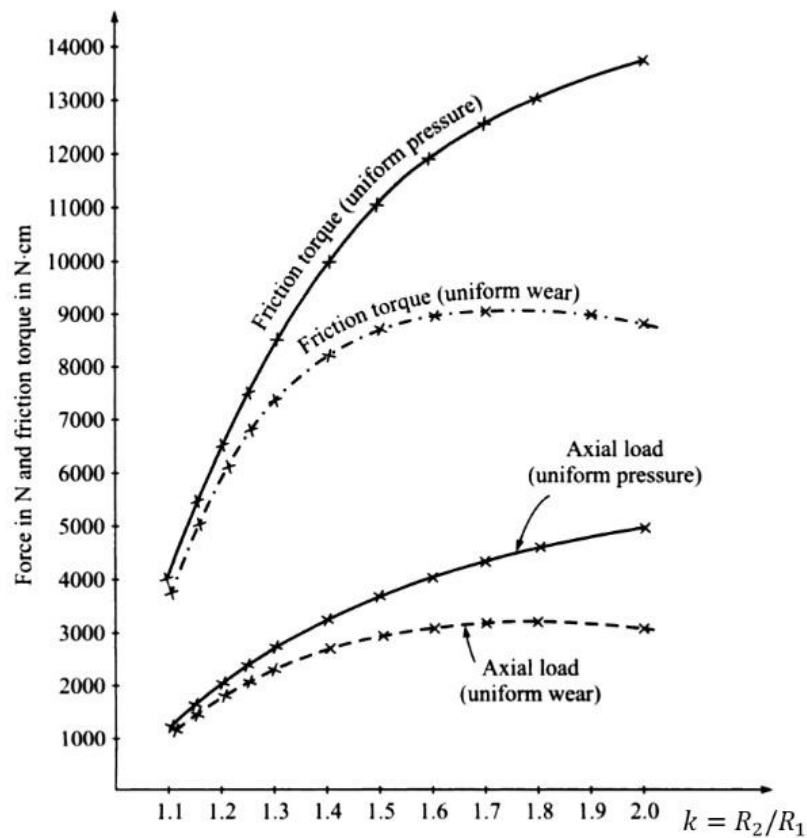


Figure 4-9 A comparison example with assumption of uniform pressure and uniform wear (courtesy of Ambekar A. G.'s book)

Once again, it can be noted from the graph that the higher amount of frictional torque in different radiuses is occurring with the assumption of uniform pressure rather than uniform wear.

As a rule, when the minimum frictional torque is desired, the assumption of uniform pressure should be considered as a conservative estimation (such as this thesis) and in contrast, when the maximum frictional torque is desired (such as power transmission capacity in clutches), the assumption of uniform wear should be selected [82].

On the other hand, one of the impacts of reaction forces can be that the two parts of the joint are pulled away from each other. The worst circumstance happens when there is a reaction force or any component force in the Z direction (Figure 4-10).

Therefore, the spring coefficient must be carefully selected in order to overcome unwanted separation from reaction forces. Note that the geometry of the conical joint can decrease separation of the joint parts as long as friction between the parts is maximized. Besides, adding rubber washers between the spring and the surroundings can remove unwanted vibrations through damping. The friction of any specific material can be varied by the amount of the normal force N . The relation between N and other parameters based on the conical joint form is formulated as shown in equation 4.48 below:

$$N = \frac{(F_{spring} + W - F_{external})}{\sin \alpha} \quad (4.48)$$

in which $F_{external}$ is the sum of Z components of all reaction forces.

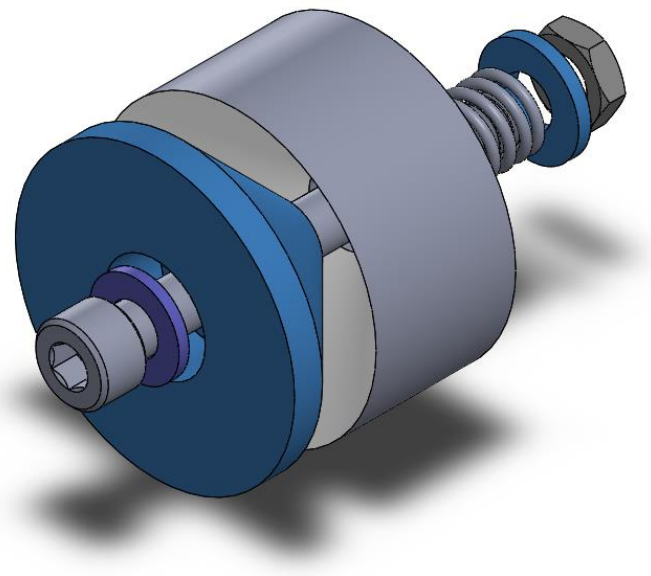
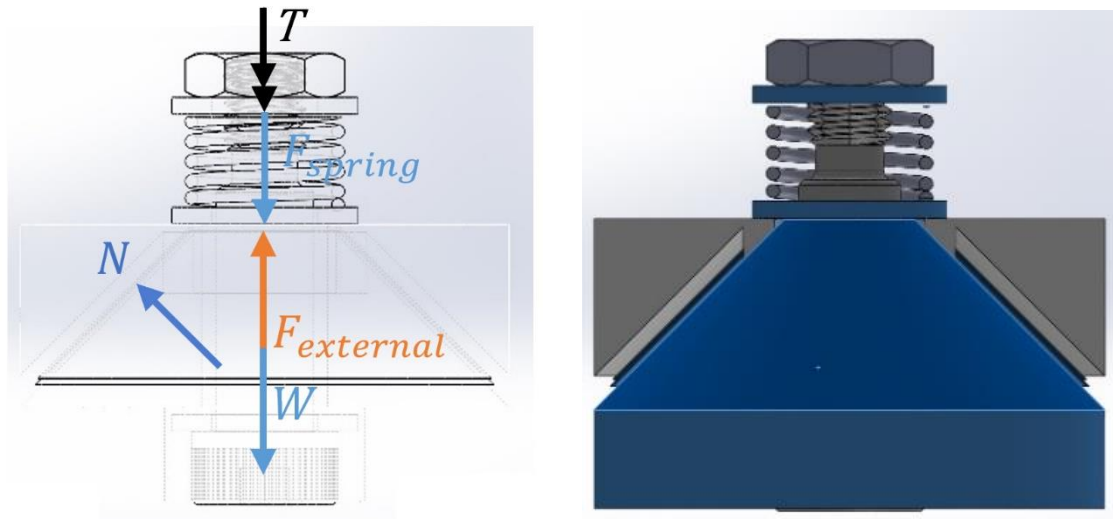


Figure 4-10 A schematic of the conical joint with external forces

As can be seen in Eq. (4.48), the taper angle affects the amount of normal force. As α approaches 0 degrees, if other variables are fixed, the normal force maximizes, which is desired in this stage.

As α approaches either 0 or 90 degrees, the joint characteristics vary such that different benefits could be utilized for specific applications. These benefits include reaching higher normal force and avoiding the parts separation with the taper angle close to 0 degrees or reaching minimum friction torque with the taper angle close to 90 degrees. Since there are two different objectives, the use of weight function can help based on the application. Eventually, the equivalence of these two targets was taken into account and the taper angle of 45 degrees was chosen in this study as a good compromise.

4.3.4. Optimization of 3D Model Case in Horizontal Direction

In many studies similar to our model [79], [80] and [81], where a similar model is utilized, the part weight of parts is neglected. This last assumption results in the fact that the direction of the model is not important whether it is vertical horizontal or diagonal. Actually, the accuracy of calculation is acceptable with a good approximation since the axial load is much more than the parts weight. An example of that is drilling machines. Looking at Table 4-3, one can realize the ratio of the weight of the upper joint parts over axial load (if we just consider the force spring without any other forces which can be added to) is around 10%. And the 10% can be neglected if the direction of the model is changed particularly when the lighter material for joint with higher spring force is used and that ratio decreases from 10% to the much small amount. Therefore, with the approximation of 10%, the calculation in any direction is the same.

In the case when the weight is concerned, the calculation for distribution of weight in horizontal direction is more complex and should be solved by software which is beyond this project.

4.4. Dry Lubricant Selection

The inner and outer joint contact surfaces can play a key role in minimizing the friction. Although oil and grease are commonly used to minimize friction at the interfaces, they are good choices for applications requiring such as working in a clean environment. Moreover, lubricant life is affected by high pressure. See the lubricant comparison results on Table 4-1 [76].

Table 4-1 Factors affecting the choice of lubricant class [76]

	Oil	Grease	Solid
Cooling	I	–	–
Availability in suitable form	I	II	–
Corrosion prevention	I	I	–
Preventing contamination of bearing	I	II	–
Time between relubrication	–	II	I

Hard vacuum	II	II	I
Very low temperature below 60 °C	–	–	I
Price	I	II	–
Minimizing wear	I	I	–
Ease of relubrication	I	II	–
Preventing contamination by lubricant	–	II	I
High temperature (above about 200 °C)	–	II	I
Friction			

1st choice I; 2nd choice II

Using a solid film is an alternative solution. There are many industrial solid film lubricants and one of the best suitable options among those is Molybdenum Disulfide (MoS₂) known as Moly [76]. From the film comparison results shown in Table 4-2, Moly is now selected for this research as it can have the least friction coefficient, be stuck to the parts very well, and have the highest PV among the others (see Table 4-2).

Table 4-2 Comparative properties of Molybdenum disulphide, Graphite and PTFE [76]

Property	Solid Lubricant		
	Molybdenum disulphide	Graphite	PTFE
Friction coefficient	0.002-0.3	0.05-0.15	0.03-0.1
Maximum PV	3.5 MPa.m/s	0.7 MPa.m/s	~60 kPa.m/s*
Thermal conductivity	Poor	Good	Very poor
Electrical conductivity	Poor to fair	Good	Very poor
Max.temp. in air, °C	350-400	540	300
Max.temp. in vacuum	650+	Not usable	Low
Adhesion	Very good	Good	Very good
Colour	Dark grey/black	Dark grey/black	White
Chemical resistance	Resistant	Resistant	Very resistant
* Increased by reinforcement to about 3 MPa.m/s, but friction is then higher			

Moly is used to coat the contact surfaces in order to decrease the friction. The reason for its very low sliding friction is due to the very low shear strength [76].

In addition of the Moly advantage of its very low friction coefficient, it has a high load-carrying capacity. Moly is often used in two-stroke engines and gears as well as used in CV (constant velocity) and universal joints [77], [78].

The use of dry lubricant could be beneficial as long as the maintenance of parts would be feasible in terms of price, time, and ease of assembly and disassembly.

Many coated contact surfaces can be repeated to achieve the minimum friction, maintenance and ease of use as it will study in the following section.

4.5. Conical Joint with Two Sleeves

4.5.1. Single Contact Surfaces

There are different methods of selecting contact surfaces and Moly coating but the question is that in which way we can achieve the minimum friction, minimum maintenance and ease of use. One of those ways is to coat Moly directly on the interface of the inner and outer joint parts. However, after a specific time which is the wear life of the solid film lubricant, the parts should be recoated again. Thus, dismantlement and removal of the joint in a mechanism, surface recoating and reinstallation can be costly and time consuming. Moreover, the mechanism shall be subject for an operational interruption until the joint is constructed and calibrated again, which is not reasonable.

4.5.2. Contact Surfaces with One Removable Sleeve

Another alternative is using a sleeve between the interface of joints and coating the two sides of the sleeve. It can be replaced any time and the second set of the coated sleeve can be used immediately which is much cheaper than changing the whole joint. The fact is that the contact areas between the sleeve and joint parts including both sides of the sleeve besides inner and outer joint parts have to be coated by Moly otherwise the friction will increase despite the fact that the sleeve is coated. The problem will appear after reaching the wear life of the Moly film. This will require that the sleeve be recoated. Moreover, there is a risk that wear may occur on joint parts thereby requiring that they should be recoated.

In other word, there is a difficulty potential arising from the use of one sleeve between the joint parts.

4.5.3. Contact Surfaces with Two Removable Sleeves

The third alternative is using two sleeves in contact with each other between the joint interface as seen in Figure 4-11 and Figure 4-12. This alternative involves the coating of the contact surfaces between these sleeves. In this case, there is no need to coat the interface of inner and outer joint parts since there is minimum friction between the two sleeves thereby allowing joint rotation.

In order to benefit from Moly coating, to reduce the friction in the joint, the sleeves are coated on the sides at the interface.

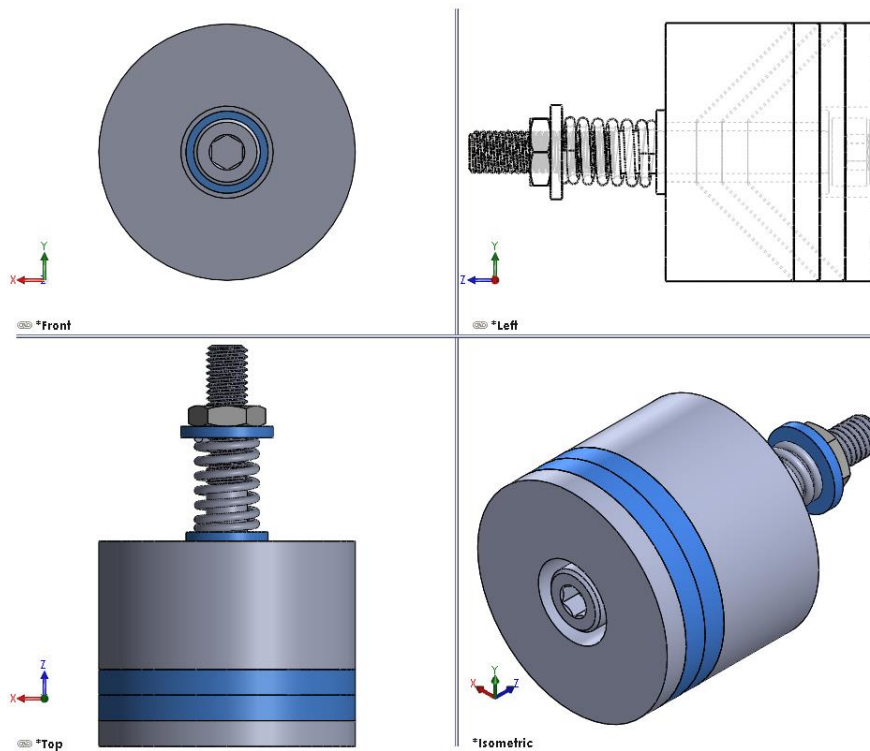


Figure 4-11 The full assembly of conical joint with two sleeves

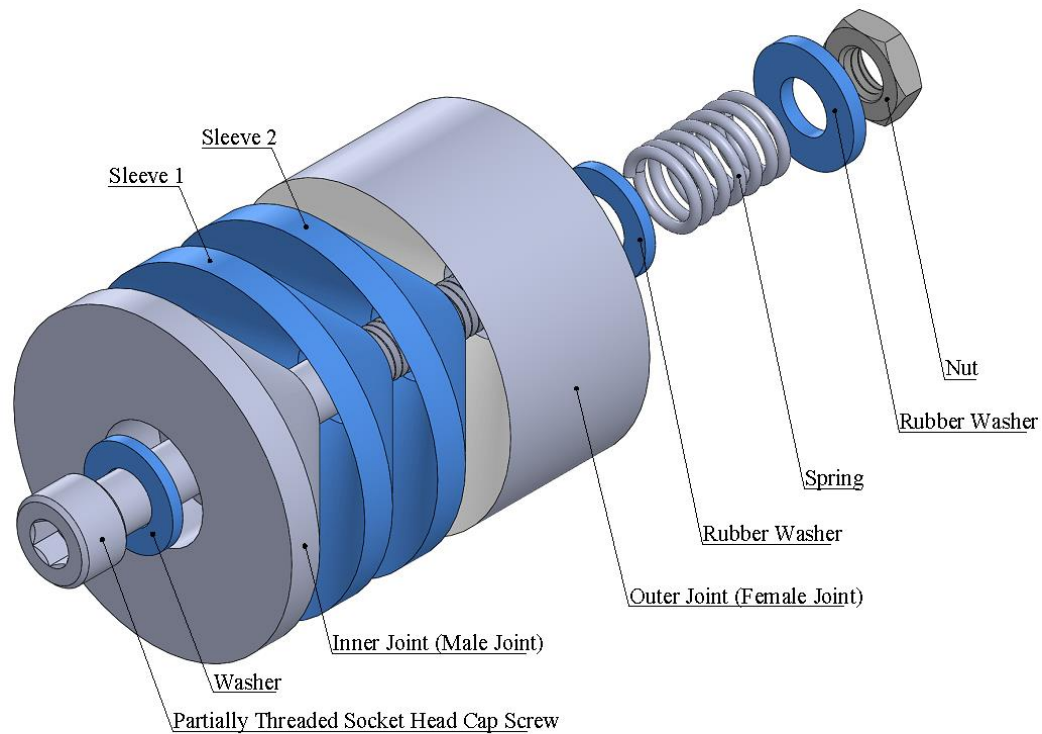


Figure 4-12 Exploded view of conical joint with two sleeves

In this case, there is no need to coat the interface of inner and outer joint parts since there is minimum friction between the two sleeves and this leads to the rotation of the joint parts.

In addition, since the thickness of sleeves is the same throughout the contact area, all the previous calculations to pick a good compromise of taper angle are valid.

There are some important advantages of using two sleeves such as the fact that making and storing the second set of sleeves has a lower cost compared to making the second set of whole joints. Therefore, while one set of sleeves is running, another set is

ready to use whenever the first set should be replaced and it also allows for better maintenance.

One may ask the question if it is beneficial to use more than two sleeves. In fact, the main reason for using two sleeves is to minimise the rotational friction. However, it should be noted that the joint parts rotate along their lower frictional surfaces (in this case, internal sleeves) and adding other sleeves cannot be helpful since the same coating with same coefficient friction is used.

4.6. Self Locking

In joints self-locking is defined as the joint positions, conditions or configurations where the actuators cannot move or rotate the joint parts around the motion axis. And it occurs when specific relationships exist between friction coefficients and mechanism kinematics are as if the actuators forces cannot overcome friction forces to move the parts [69], [70].

The self-locking principle is a common phenomenon which can be either useful (such as self-locking fasteners) or undesirable in mechanisms (such as the current revolute joint) depending on the applications. Therefore, according to its role, the calculation should be performed [71][72][73][74][75].

Finding the necessary torque to prevent the self-locking is subject to the definition of all variables from equation 4.24.

To have a demonstration and also functional test, the following values and dimensions were selected:

Table 4-3 Values and dimensions of the conical joint

The compressed length of spring	0.21 inch or 5.334 millimeter
Constant of spring k	52.34 <i>lbs/inch</i> or 9.166 <i>N/mm</i>
The force spring	48.891444 <i>N</i>
The weight of the upper joint parts	4.886 <i>N</i>
The static coefficient of Moly μ_s	0.08
R_2	25 <i>mm</i>
R_1	6 <i>mm</i>
α	45°

From equation 4.24, we result in:

$$T = \frac{2}{3} \frac{0.08 \times (48.891444 + 4.886)}{\sin 45} \left[\frac{25^3 - 6^3}{25^2 - 6^2} \right] = 106.114 \text{ N} \cdot \text{mm}$$

And from equation 4.25, we result in:

$$T = \frac{1}{2} \frac{0.08 \times (48.891444 + 4.886)}{\sin 45} (25 + 6) = 94.3055 \text{ N} \cdot \text{mm}$$

The minimum torque amount of 106.114 *N.mm* is considered to yield a conservative result. In other words, an external torque greater than 106.114 *N.mm* can rotate the joint and one lesser amount encounters the self-locking condition.

Chapter 5

Chapter 5: Manufacturing and Result

5.1. Manufacturing

The new conical joint using two sleeves was fabricated in the machine shop of Tech Services at Memorial University (Figure 5-1). The sleeves were produced by Lathe machine with fine surface finishing and the outer and inner joints were produced by CNC milling. The bolts, rubber washers, spring and stainless steel washer were ordered from mcmaster.com. Because of the shape of the joint parts, all parts can be easily assembled without any loose and can be fitted easily in their positions. The prototype can be also easily disassembled and the various parts are shown in Figure 5-2. The outer part of the joint was produced in such a way that it can be attached to the stand of 3-RPR planar parallel robot at the High Performance Robot Lab at Memorial University, see Figure 5-3. The parts confirm the feasibility of joint sleeve replacement since it only takes unscrewing one bolt holding the spring and then the joint is disassembled.

It should be mentioned that the axial force is the force spring and the weight of the joint, also there is no external force resulting from vibration or other unwanted sources in Z direction in our robot. In addition, the total axial force was less than 10 N (2.25 lbs). Moreover, the spring displacement with the constant k of 9.166 N/mm (52.34 lbs/inch)

and the max load of 70.68 N (15.89 lbs) was set to 70% of the maximum static compression displacement.

Adding rubber washers to the beginning and end of the spring were introduced to provide for damping of any unwanted axial force which can cause interface separation, vibration and impacts on the joint parts.

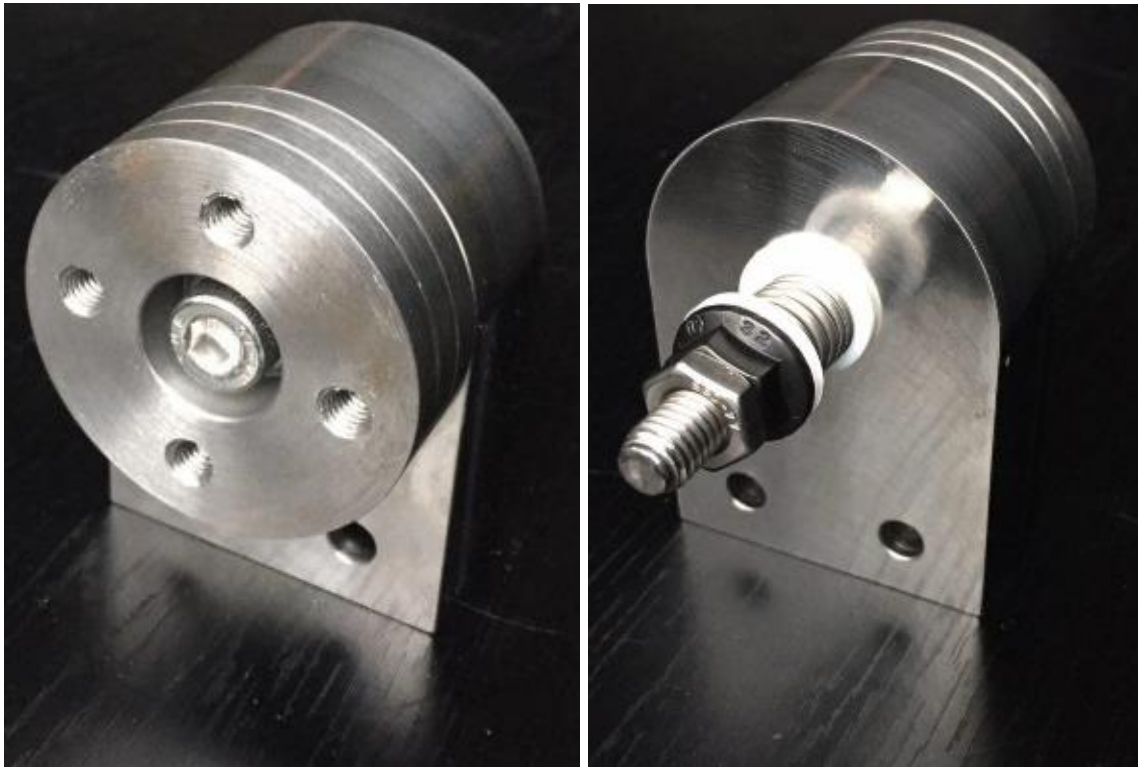


Figure 5-1 The conical joint assembly as a rigid revolute joint



Figure 5-2 The conical joint parts



Figure 5-3 The fabricated conical joint installed on the 3-RPR planar parallel robot at the High Performance Robot Lab at Memorial University

5.2. Results and Discussion

In this work, a novel revolute joint with extremely rigidity was produced and fabricated. The whole joint can tolerate significant axial pressure loads due to the smart shape of the joint parts without any complexity or vulnerable piece.

The friction and torque at start-up were investigated. In addition, the conical taper angle was determined. The taper angle was selected as a good compromise (45 degrees) of both avoiding the separation of joint parts goal and also minimize the friction torque purpose.

The conical joint was produced implementing two sleeves. These are completely removable and it is also possible to test the conical joint without any sleeves or with just only one. The sleeves were added to reduce the joint interface friction with the goal of approaching zero friction. The percentage of 36% was deducted from the rotational friction in mirror finish stainless steel parts after using Moly (full calculation comes out in next chapter). It shows the effect of the Moly to reduce the friction even compared to the stainless steel material with mirror surface finishing (with a grade of AAA which means the flatness of up to 250 nm). If the surface finishing of the original material is not as great as AAA, the amount of deduction of friction with using Moly will be even much higher and it can be seen the effect of Moly.

This would benefit the common revolute joint design by reducing the stress on the contact area compared to the similar ball bearings or roller bearings while it keeps the

friction at a relatively low level. Reduction of the interface stress is through the interface surface increase.

In addition, the proposed design met the self-centering factor.

Consequently, the backlash problem has been solved in all instances and should not appear since the joint is self-centering.

Furthermore, using Moly in contact with the inner joint parts benefits from smooth contact surfaces with the role of a sacrificial element in compared to stainless steel. And results in zero-clearance approach as one of the desired factors of our joints.

Finally, the sleeves can function as a mechanical fuse whereby if the rotary contact surfaces fail, another set of sleeves will be installed instead of changing the whole joint, which is more cost-effective. Besides, they can be used to as the surfaces where wear is going to appear as a result of friction. It is thus possible to mitigate the effects of joint wear by attracting the wear to the sleeve.

Chapter 6

Chapter 6: Verification

There are different functional tests which could be carried out. One of the important tests is to measure the joint interface friction. These tests should be performed with and without coating the sleeves with Moly and compare their results in order to examine the effectiveness of using the dry lubricant as the means to reduce transmitted torque through the revolute joint being one of the performance requirements and ultimately achievements in this design.

Measuring the wear and evaluating fatigue tests were left for further studies since they involve acquiring appropriate testbeds.

6.1. Method of Verification

There are different methods to measure the friction. As a state-of-art, here is a list with their brief summary. The following section will provide the friction test with the method that was selected (with the courtesy of tribology-abc) [87].

6.1.1. Method 1 Weight Ratio

Leonardo da Vinci (ca. 1500) studied friction by hanging weights from one side of a desk (as it can be seen from the figure) and connecting to the mass which would find the coefficient friction or friction force. The mass has to be placed in a flat and horizontal surface.

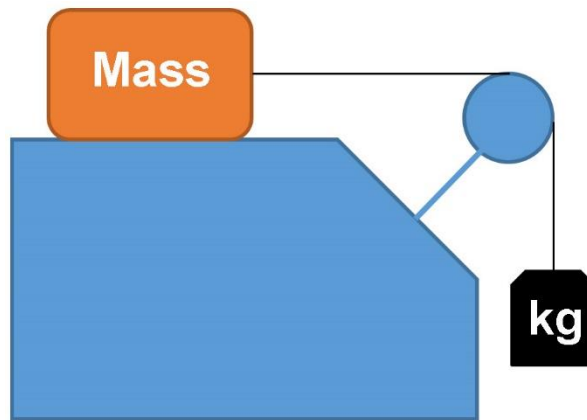


Figure 6-1 Schematic diagram of static frictional test setup - weight ratio method

$$\mu = F_f / N = m_{\text{weight}} / m_{\text{Mass}} \quad (6.1)$$

where F_f is the frictional force of the Mass and N is the normal force applied to the Mass.

The experiment set-up comprises a mass, a weight plate and a pulley all installed on a table.

The experiment starts with a small amount of weights selected so to make sure that the mass remains statically stable without any movement. Then, small weight increments are gradually added to the weight plate until the mass starts moving. This moment

corresponds to start which is determined by static friction before friction becomes dynamic and similarly, this gives the static coefficient friction of the mass.

When the mass commences sliding continues, the static friction converts to dynamic or kinetic friction. The amount of dynamic friction is usually lower than static friction for any particular material. After continuous sliding, the amount of force measurement on the spring balance shows the dynamic friction.

Besides, the static friction coefficient is dependent on contact pressure, temperature, and surface finishing. The contact pressure is proportional to the mass weight or the reaction force at the interface between the mass and the table surface.

6.1.2. Method 2: Spring Balance



Figure 6-2 Schematic diagram of static frictional test setup - spring balance method

The measure of friction can be done by connecting a spring balance to a mass located on a horizontal surface.

The spring balance should be gradually pulled and this process results in spring extension without any mass motion. The operator raises the spring force until the mass starts sliding.

$$F_{spring} = K e \quad (6.2)$$

$$\mu = F_{spring}/N = F_{spring}/(m_{Mass} \cdot g), \quad g=9.81 \text{ m/s}^2 \quad (6.3)$$

where K is the spring constant where a linear spring is assumed and e is the measured spring extension.

The amount of force measurement on the spring balance at the moment that sliding begins is the static friction. And after continuous sliding, the amount of force measurement on the spring balance shows the dynamic friction.

6.1.3. Method 3: Tilted Plane

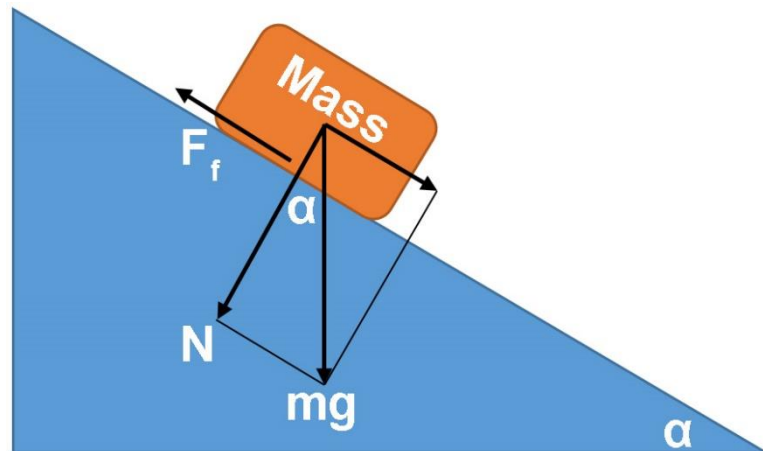


Figure 6-3 Schematic diagram of static frictional test setup - tilted plane method

If the mass is placed on a tilted surface and the angle of surface is increased from the horizontal position (0 degrees) until when the mass starts sliding, the tangent of the surface angle is equal to the static coefficient of friction.

$$\mu = \tan \alpha = F_f/N \quad (6.4)$$

where α is the angle of the tilted plane.

6.1.4. Method 4: Clamping



Figure 6-4 Clamping the object with high contact pressure (courtesy of toolmonger) [88]

The mass may be put under high contact pressure with another surface such as in a light clamp. The force required to overcome the friction and move the mass must be halved after measurement since the surface under high pressure condition would double the total friction.

6.1.5. Method 6: Motorized Tribometers

Tribometers are special devices to measure the coefficient of friction, friction force, and wear volume between two contact surfaces.

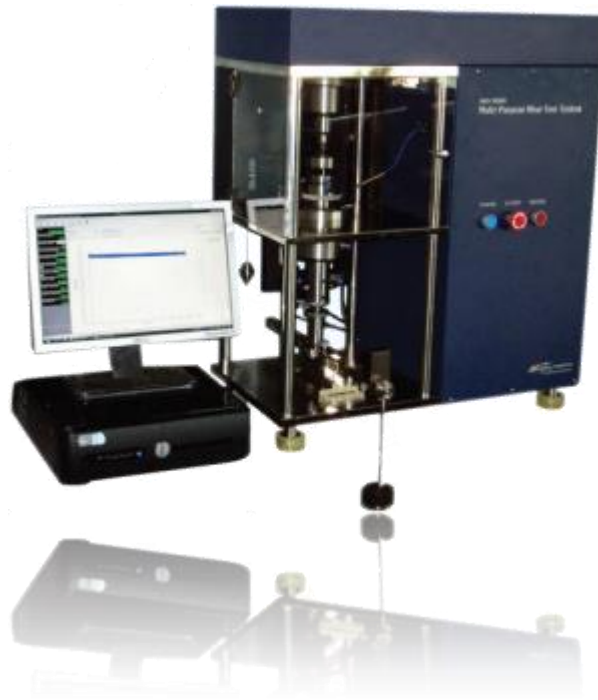


Figure 6-5 Multi-Purpose Wear Test System / MPW110 / Friction and Wear Testing - LPR Global, Inc. (courtesy of uskoreahotlink) [89]

Although more precise, this approach is very expensive. It should be mentioned that the coefficient of friction can be subject to variations after some hours of working (sliding or rotating) on contact surfaces. A tribometer is specialized to measure and show the wear rate and the contact temperature over a period of time and also the necessary time needed to measure the friction coefficient when stability is reached.

6.2. Bed Testbed Structure and Results

The method of weight ratio was selected to measure the friction. In this regard, the revolute joint was placed in vertical direction. A thin cable was inserted through the hole at the end of the upper part and the lower part was tightened with a work vise. The other side of the cable was attached to a scale after rotation of 90 degrees around a very low friction pulley. The route of the cable was completely horizontal and vertical, Figure 6-6 and Figure 6-7.

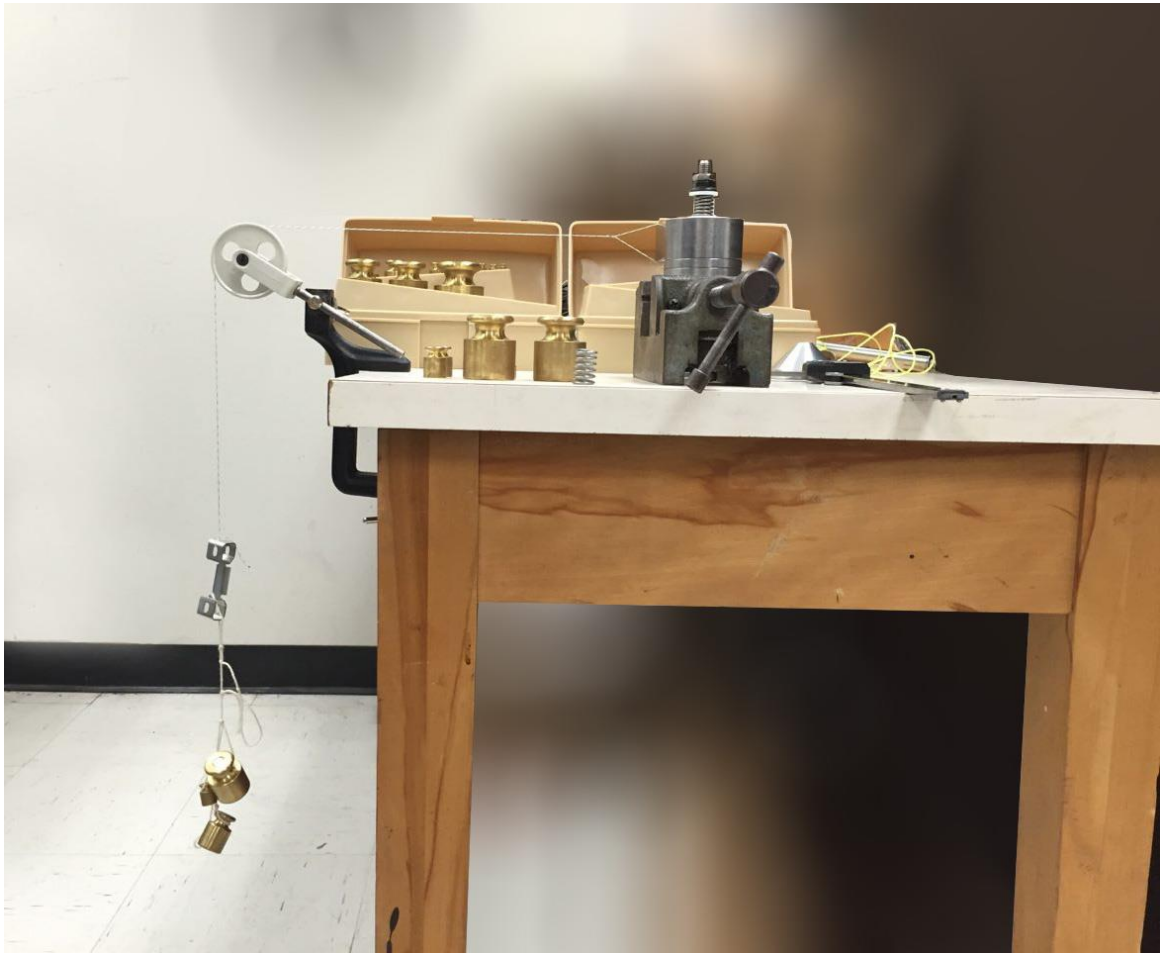


Figure 6-6 The bed test structure and the position of the parts from front view



Figure 6-7 The bed test structure and the position of the parts from top view

The necessary force and then after the static friction was found after adding enough weights when the motion of the joint upper part just started. If the weights are directly hanged to the weight hanger, inaccurate result may be created. The reason is the difference

between the impact force of falling a mass (dynamic) and its weight in static mode in which the amount of impact force in dynamic mode is different with the weight in static mode. Therefore, in order to reach more accurate results, the upper part of the joint was held in position with one hand and after adding any amount of weight, it was gradually released to see whether it started rotating or not.

Testing and finding the static friction was done for every 10 degrees circular pattern of upper joint part. Eventually the average of $(360^\circ/10^\circ=36)$ times was defined for both before and after coating Moly with the same condition of static forces. Table 6-1 shows the results.

Table 6-1 The verification result with ± 1 gram tolerance

	Mirror finish stainless steel	With Moly
Average force	39 <i>gf</i> (0.3826 N)	25 <i>gf</i> (0.2453 N)

Therefore, we know that the *Torque* can be determined by equation 6.5:

$$Torque = F \times r \quad (6.5)$$

where, F is the force vector and r is the position vector where is a minimum distance of the axial rotation on the revolute joint and the direction of the applied force F .

Before coating Moly:

The minimum rotational torque for mirror finish stainless steel is:

$$T = 0.3826 \times 35 = 13.3907 \text{ N.mm}$$

If T is substituted in equation 4.24, this gives us:

$$T = 13.3907 = \frac{2}{3} \frac{\mu_s \times (4.886)}{\sin 45} \left[\frac{25^3 - 6^3}{25^2 - 6^2} \right] \text{ N.mm}$$

The μ_s result for mirror finish stainless steel is:

$$0.1111$$

From 4.48, we have:

$$N = \frac{(4.886)}{\sin 45} = 6.9099 \text{ N}$$

From 4.3, the minimum rotational friction force is

$$f = 0.1111 \times 6.9099 = 0.7678 \text{ N}$$

After coating Moly:

The minimum rotational torque for Moly is:

$$T = 0.2453 \times 35 = 8.5838 \text{ N.mm}$$

If T is substituted in equation 4.24, this gives us:

$$T = 8.5838 = 2/3 \frac{\mu_s \times (4.886)}{\sin 45} \left[\frac{25^3 - 6^3}{25^2 - 6^2} \right] N.mm$$

The μ_s result for Moly is:

$$0.0712$$

From 4.3, the minimum rotational friction force is equal to:

$$f = 0.0712 \times 6.9099 = 0.4922 N$$

The results show the success of using Moly as the dry lubricant to minimize the friction and transmitted torque (the essential force to rotate the upper part of 25 *gf* and 8.5838 *N.mm* of transmitted torque with Moly versus 39 *gf* and 13.3907 *N.mm*, respectively, in mirror finish stainless steel). In other words, there is a percentage of 36% reduction in the friction and transmitted torque. Here, the Moly was compared to the mirror finish stainless steel which is very smooth and has a low coefficient friction. Now if another material is used instead of steel such as aluminum, the friction coefficient will increase and its difference with Moly will rise.

The brief results come in table below:

Table 6-2 The final verification and comparison results

	Mirror finish stainless steel (before coating)	Moly (after coating)
Force to rotate the upper part	39 <i>gf</i> (0.3826 N)	25 <i>gf</i> (0.2453 N)
The minimum rotational torque	13.3907 <i>N.mm</i>	8.5838 <i>N.mm</i>
The resulted μ_s	0.1111	0.0712
The minimum rotational friction force	0.7678 <i>N</i>	0.4922 <i>N</i>
% torque/force reduction	36% 	

Chapter 7

Chapter 7: Fork Revolute Joint

The fork revolute joint is another type of the revolute joint which was already discussed in previous chapter. The difference is that in the fork revolute joint, the shaft or the cone towards the axial axis (Z direction) would be constrained by the rest of the bar (link) from both sides (Figure 7-1).

This kind of joint is more useful when there are any wanted or unwanted axial load such as carrying the weight of other mechanism parts on its each link.

Another advantage consists in maintaining collinear the two linkages.

The other advantage is that the translational load is transferred from one link to the next through two identical branches, distributing the forces. This alleviates the uncentered problems of the former design by preventing a load torque perpendicular to the joint fork plane. This will prevent certain rotational deformations.

Therefore, it can be more to prevent joint separation along the Z axis.

Nevertheless, it needs more space to assemble rather than the former revolute joint.

Hence, selection between revolute joint and fork revolute joint should be made based on the application and condition and the structure is more complex which should be used in a right application.

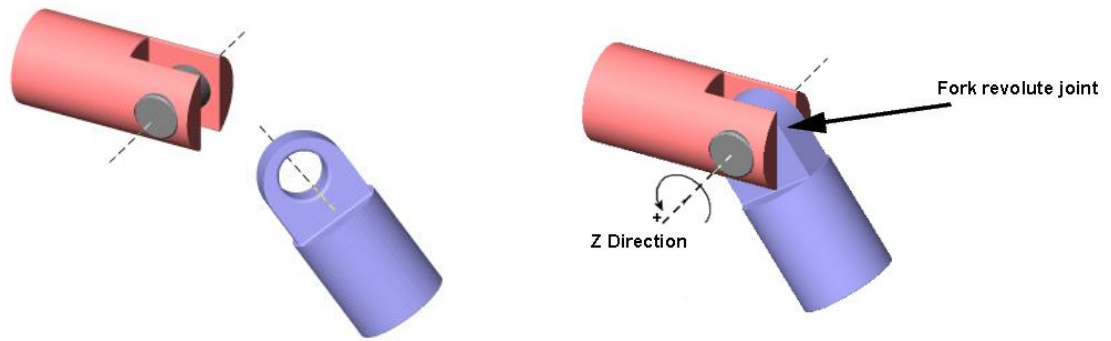


Figure 7-1 A schematic of a fork revolute joint (courtesy of mathworks) [90]

7.1. Design

The geometrical shape of the fork revolute joint should be achieved in such a way to meet the same discussed criteria:

- a) Self-centering and self-aligning
- b) Minimizing friction
- c) Minimizing backlash
- d) Maximizing rigidity
- e) Restraining the internal joint parts from two sides

Having investigated the matter, the model was designed as follows:

- The cone surfaces are facing each other
- Each cone has its own spring for adjusting itself as it was done in the former design
- The distance between the cones will be adjusted by the springs and nuts and will correct all defects and imperfections
- The cone distance being non-fixed requires that the second fork branch be adjustable to accept the variable cone separation even if the variations are very small, the goal is to avoid bending the fork also avoiding to bring transverse loads and torques on the cones
- The second branch was added making shear transmission of link translations, X axis torque transmission and Y axis torque transmission

One of the important point in this design was avoiding shapes with sharp edges which helps reducing stress concentrations and fracture or metal fatigue.

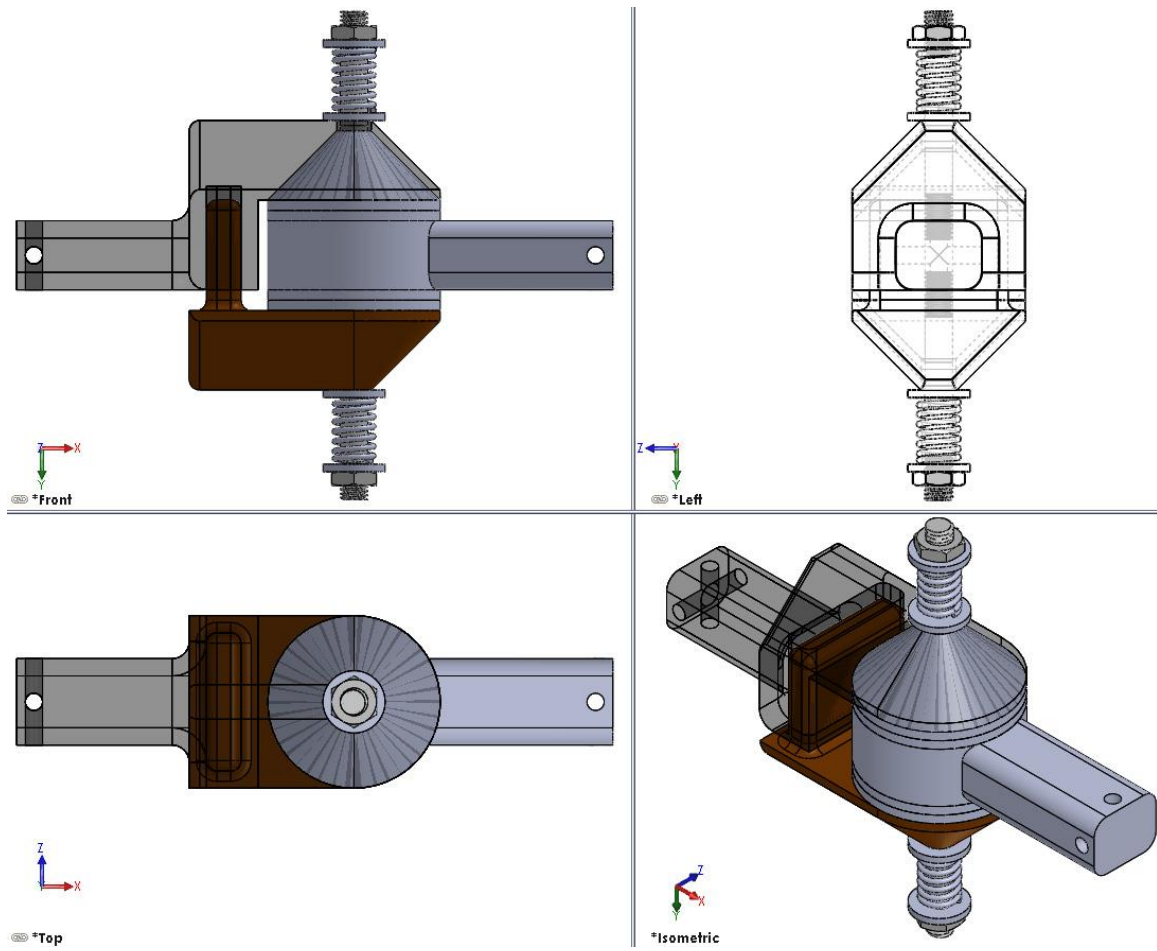


Figure 7-2 The full assembly of fork revolute joint

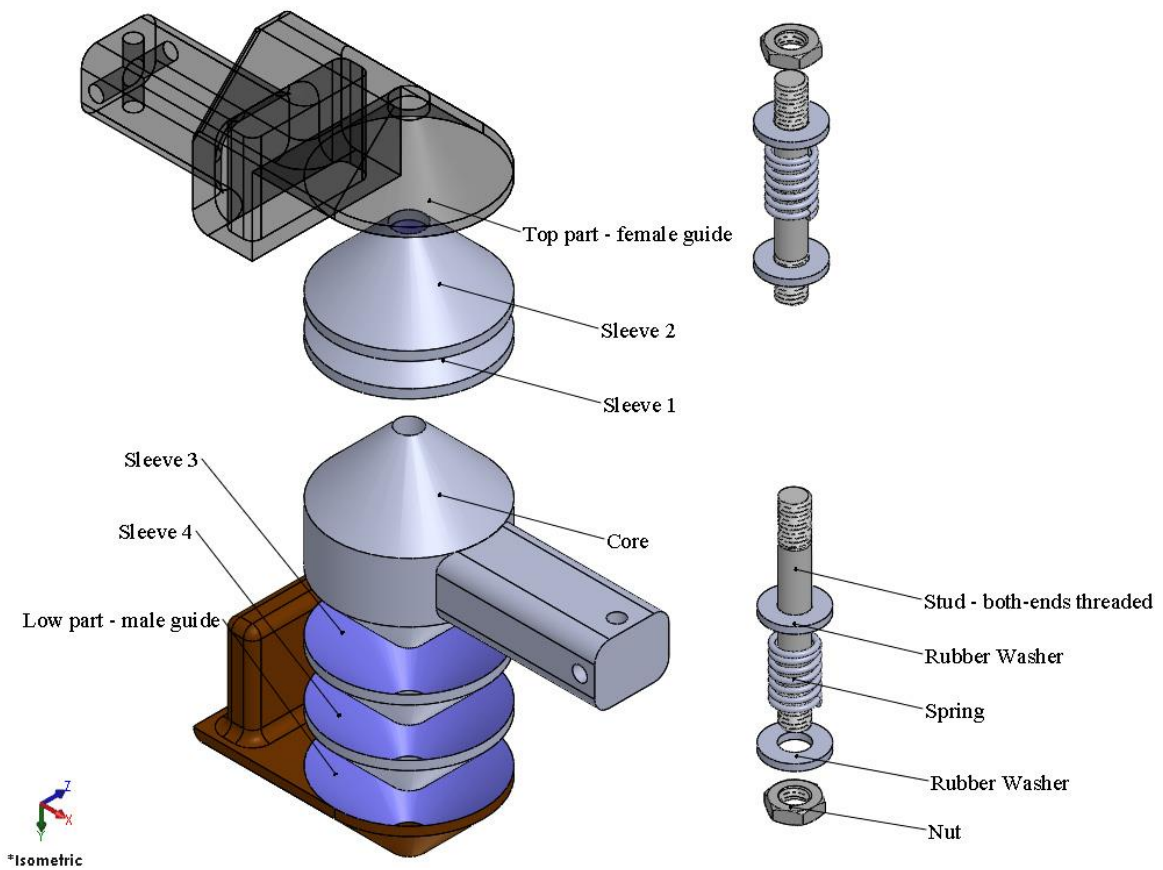


Figure 7-3 Exploded view of fork revolute joint

7.2. Manufacturing

The fork revolute joint using sleeves was fabricated in the machine shop at Memorial University (Figure 7-4).

Construction only required the doubling of the former revolute joint as it is the case with fork revolute joints.

The only construction addition is the slide that was introduced for one side to make sure that the cone distance variations could be accepted.

The slide clearance formed a tight fit of 5 μm . If the clearance fit is larger, then the entire fit would be free with movement due to its loose and therefore less reliable.

Again, it is easy to assemble and disassemble the fork revolute joint by unscrewing the joint screws simplifying maintenance over traditional fork joints.

Added complexity in construction is compensated by maintenance simplification.

The two cones are kept identical allowing design simplicity with a lesser number of part types by repeating them.

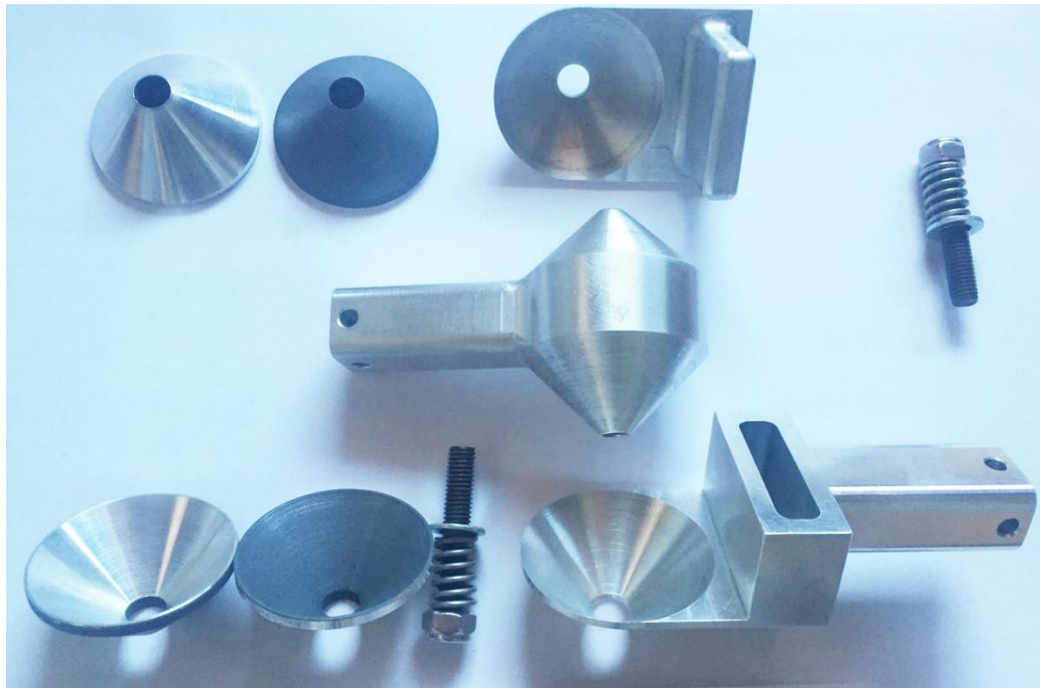
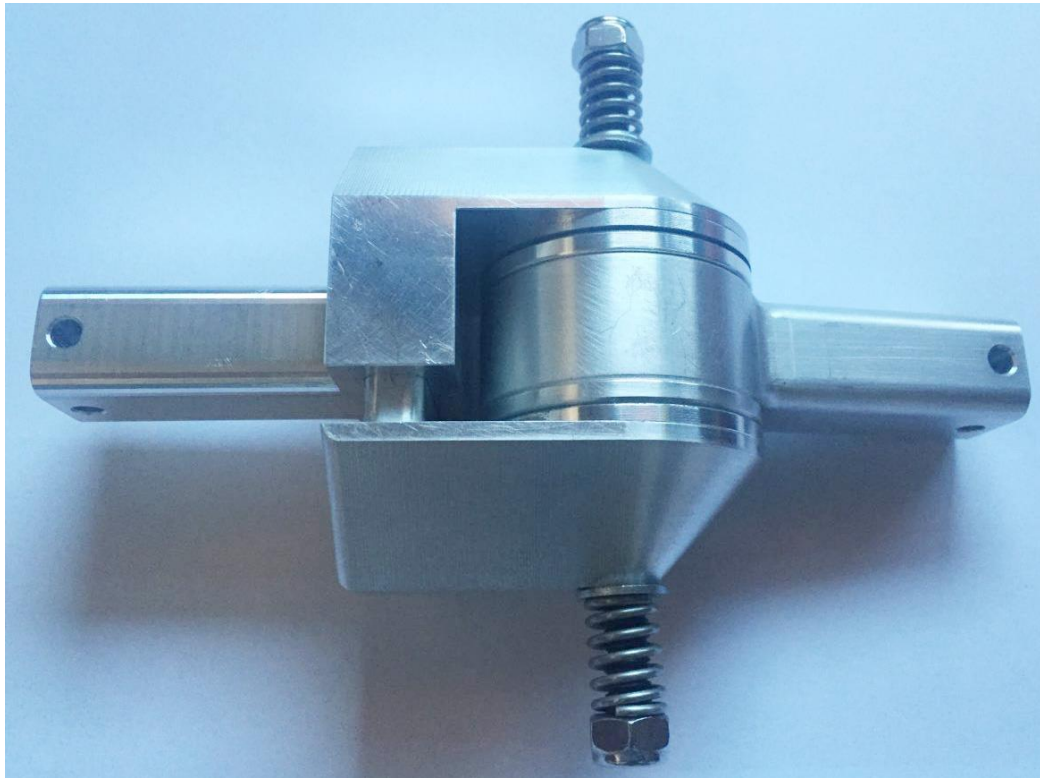


Figure 7-4 The fabricated conical fork revolute joint using sleeves

Chapter 8

Chapter 8: Universal Joint

A universal joint is a joint with 2 rotational degrees of freedom which was introduced in section 2.1.2. The main purposes are transferring torque or power from one shaft to another shaft.

In robotics, which involves mechanism design where there is a need for an interface between two linkages, this joint freely allows two rotations between the two linkages being done by constraining the pair in the three translations and one rotation.

This is particularly useful in parallel robots such as the Gough-Stewart platform being utilized as the motion base for flight simulators.

Universal joints can be used whether single or double in industry (Figure 8-1). Having the universal joint with high rigidity and low back lash would notability assist the mechanism improvement.

If there is not enough lubrication and also proper sealing of the joint parts, the life time of the parts would dramatically decrease by corrosion which results increase in wear [91]. Therefore, with the improvement of adequate lubrication and suitable sealing, the life time of the joint can only be limited by fatigue of the material in a long term [91].



Figure 8-1 Universal joints by Belden Universal Co. (courtesy of beldenuniversal) [92]

a) Single Universal Joints

b) Double Universal Joints

The same list of performance criteria for the design of the revolute joint was applied to the Universal joint. As a reminder, they are:

- a) Self-centering and self-aligning
- b) Minimizing friction
- c) Minimizing backlash
- d) Maximizing rigidity
- e) Restraining the internal joint parts from two sides

8.1. Design

In most Universal joints, they extrapolate the fork revolute to two DOFs. Here, the same method for the same reasons to take advantage of the revolute joint has been done.

In order to reach the discussed criteria such as enough lubrication and proper sealing of the joint parts as well as all the desired factors which were already investigated for the revolute joint, the design of universal joint is represented as the combination of two fork revolute joint which gives two degrees of freedom with the rotation of two perpendicular axes (RR). The following figures show the design.

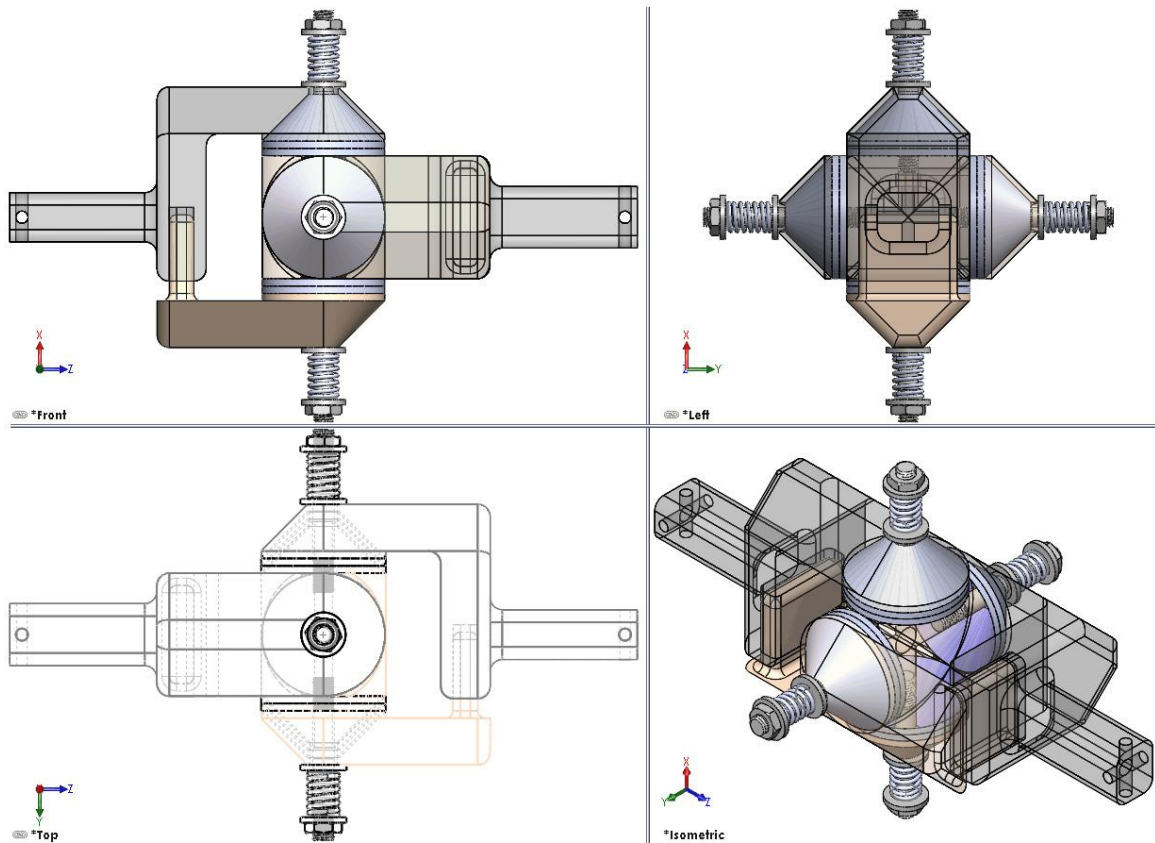


Figure 8-2 The design and full assembly of universal joint

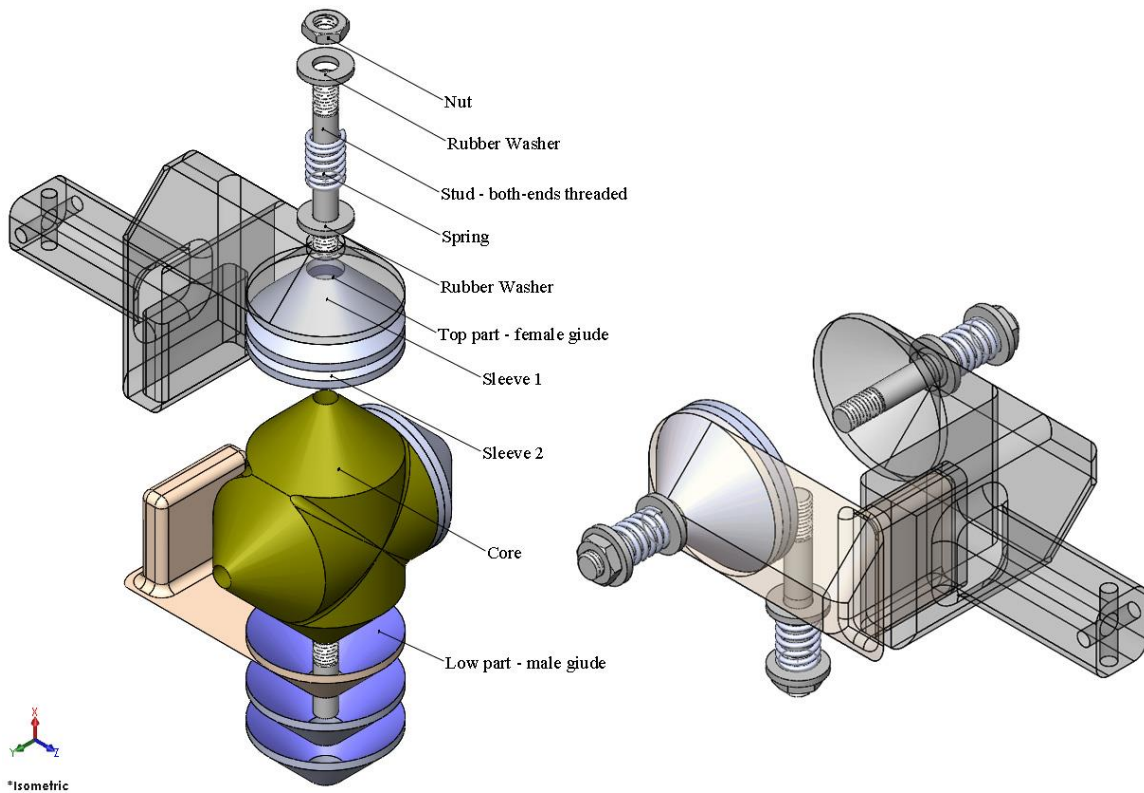


Figure 8-3 Exploded view of universal joint

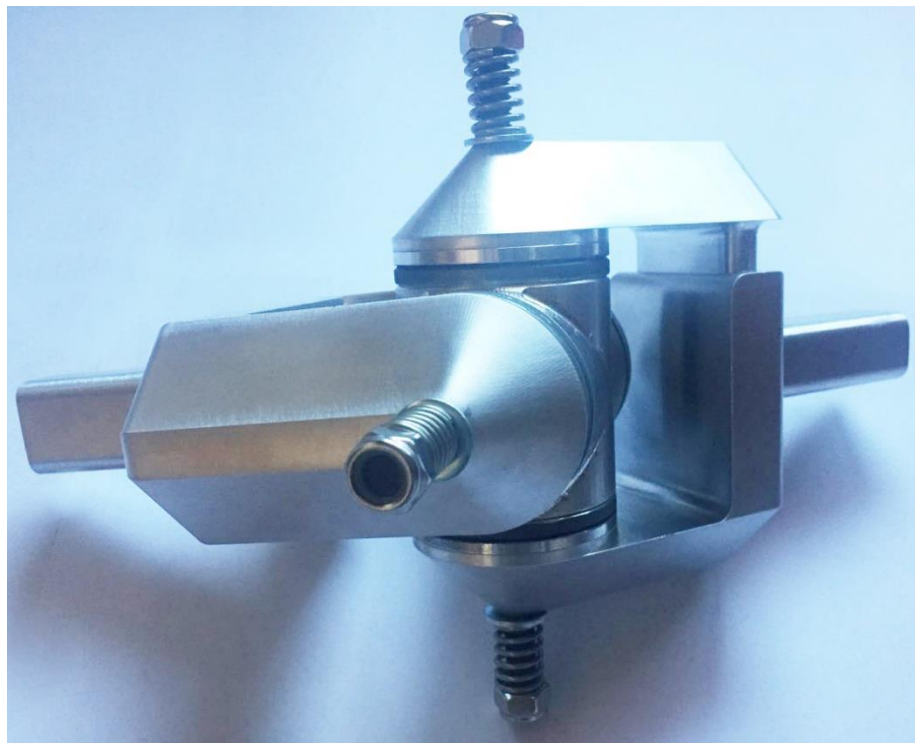
8.2. Manufacturing

The universal joint using sleeves was fabricated in the machine shop at Memorial University (Figure 8-4).

Construction only required the doubling of the former fork revolute joint as it is the case with fork revolute joints. The only difference is that the block that used to contain two

cones now is becoming one block with four cones being located perpendicular to each other on one plane. The fork parts remain unchanged and completely interchangeable.

This allows interchangeability which is simplifying construction with a lesser number of part types by repeating them. Again, it is easy to assemble and disassemble the Universal joint by unscrewing the joint screws simplifying maintenance over traditional fork joints. Added complexity in construction is compensated by maintenance simplification. The two cones are kept identical allowing design simplicity.



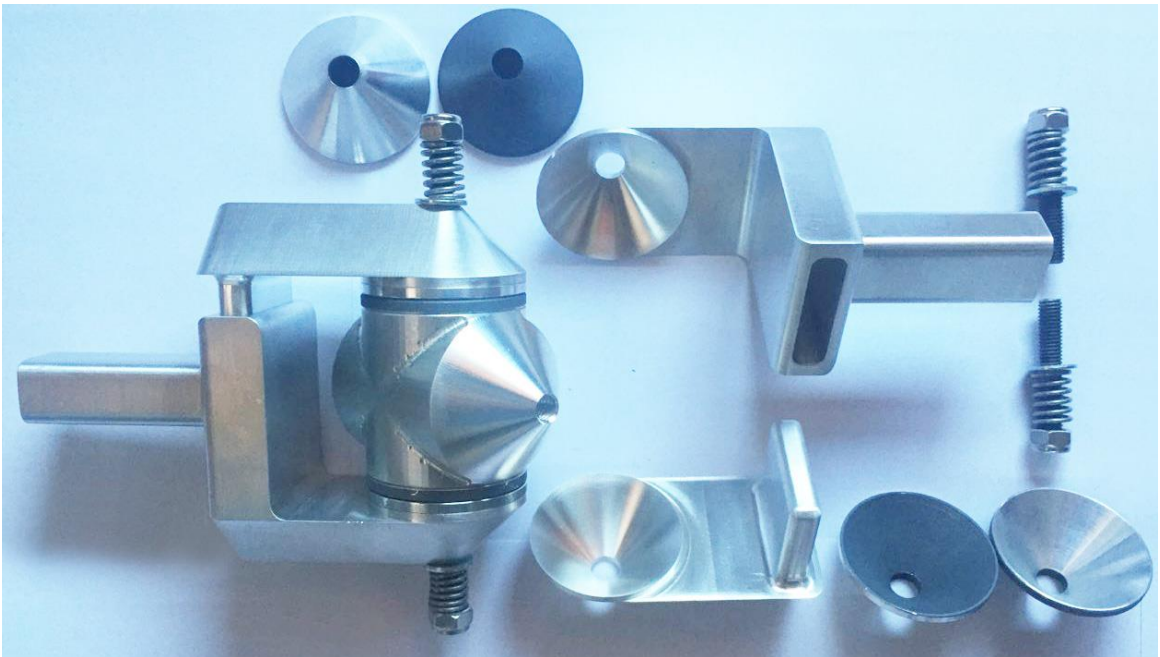
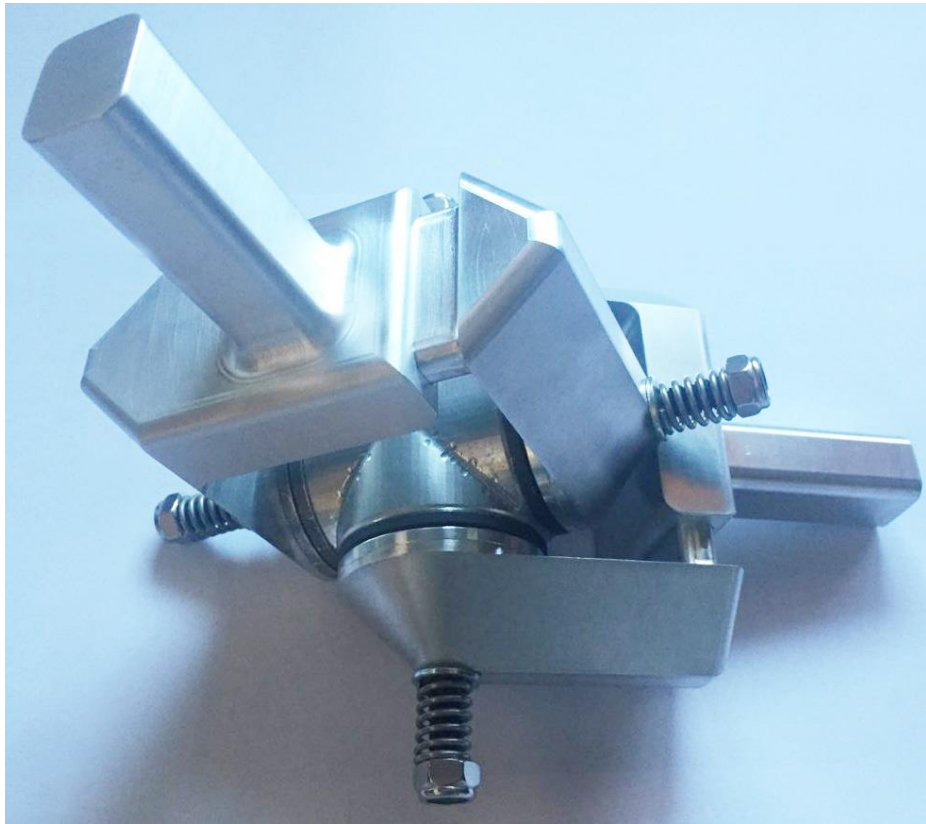


Figure 8-4 The fabricated universal joint using sleeves

Chapter 9

Chapter 9: Ball Joint

A ball or spherical joint, is a joint with 3 rotational degrees of freedom which was introduced in section 2.1.3.

In robotics, which involves mechanism design where there is a need for an interface between two linkages, this joint freely allows the three rotations to occur between the two linkages being done by constraining the pair in the three translations only. The important specific challenge of these is the fact that rotation ranges are very limited and would make them unsuitable for parallel mechanism applied as solar tracker for example. This is particularly useful in parallel robots such as the Gough-Stewart platform being utilized as the motion base for flight simulators. The same list of performance criteria for the design of the revolute joint was applied to the ball joint. As a reminder, they are:

- a) Self-centering and self-aligning
- b) Minimizing friction
- c) Minimizing backlash
- d) Maximizing rigidity
- e) Restraining the internal joint parts from two sides

Angular capability, limit on the range of motion and ball-retention capability of ball joints have been always critical problems and challenges in terms of theory as well as fabrication [93].

In addition to all the criteria which have been the main factors in this thesis, the capability of full range of motion in ball joint would be a remarkable improvement.

9.1. Design

To reach the large range of motion in the ball joint as well as complete ball retention capability, the combination of three revolute joint was considered in such a way that the mechanism fulfills three degree of freedom (RRR) in concentric manner. Fortunately, it could be reutilized the former fork-based Universal joint along with the fork-based revolute joint replacing an S joint by a geometrically equivalent UR one.

Following design shows how the ball joint can reach a large range of motion (Figure 9-1 and Figure 9-2). One of the achievements of this design is to reach over 180 degrees motion in any axis of rotation with extending the fork part (Figure 9-3). The fork lengths are increased allowing the center square shape block to rotate inwards even to the point of clearing the screw lengths from collisions with the fork bottom. The screw lengths will determine the fork extensions. Note that the third rotation is allowing unlimited joint rotation. Also note that the proposed joint provides for a redundant third rotation which could be restrained to only one.

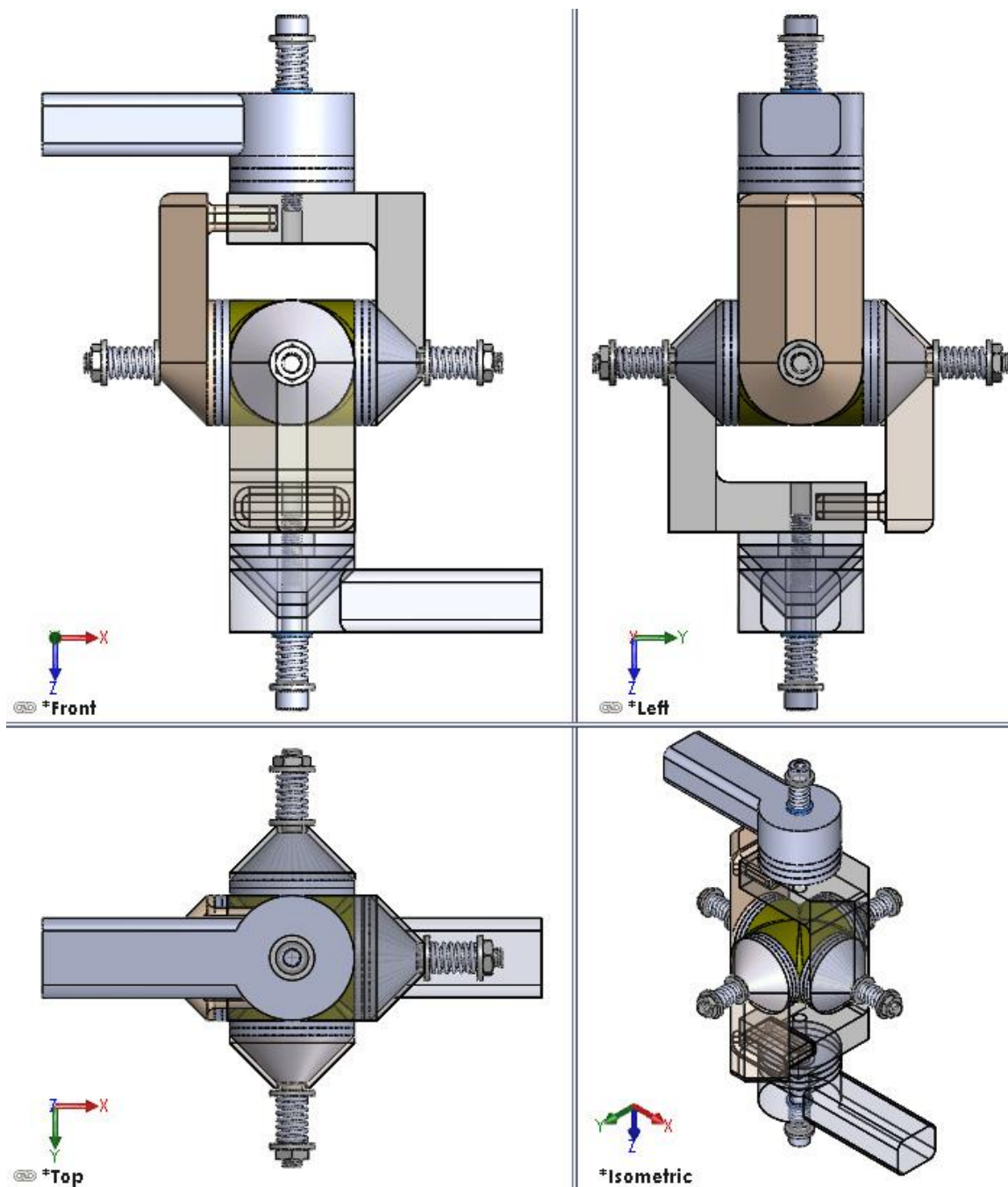


Figure 9-1 The design and full assembly of the ball joint

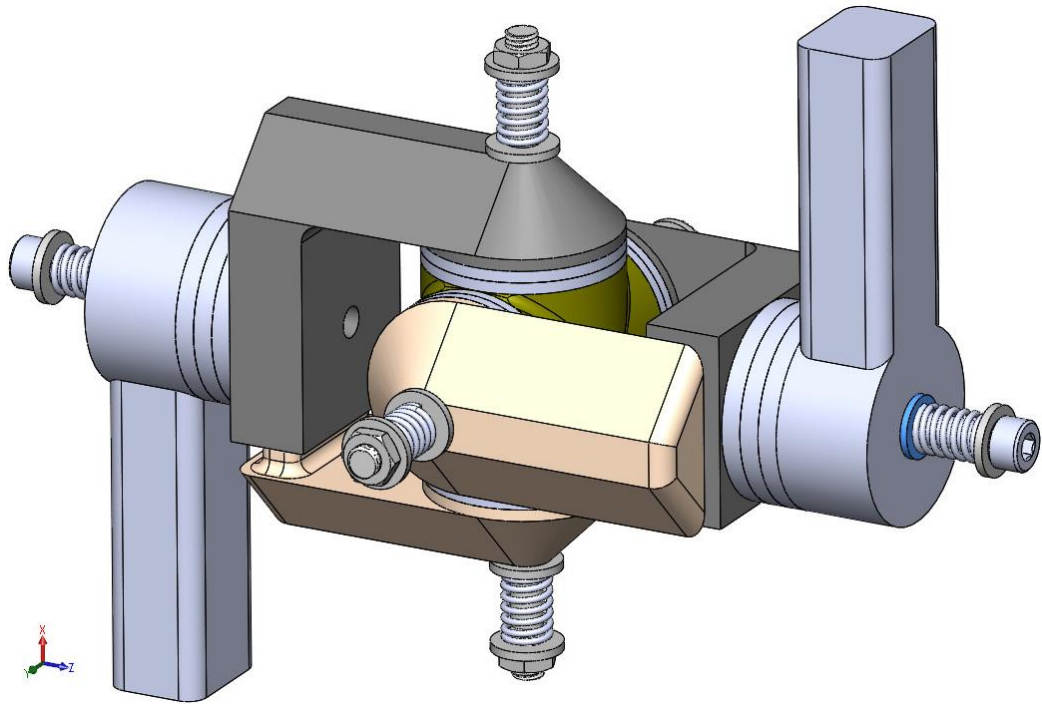


Figure 9-2 A larger view of the ball joint (RUR)

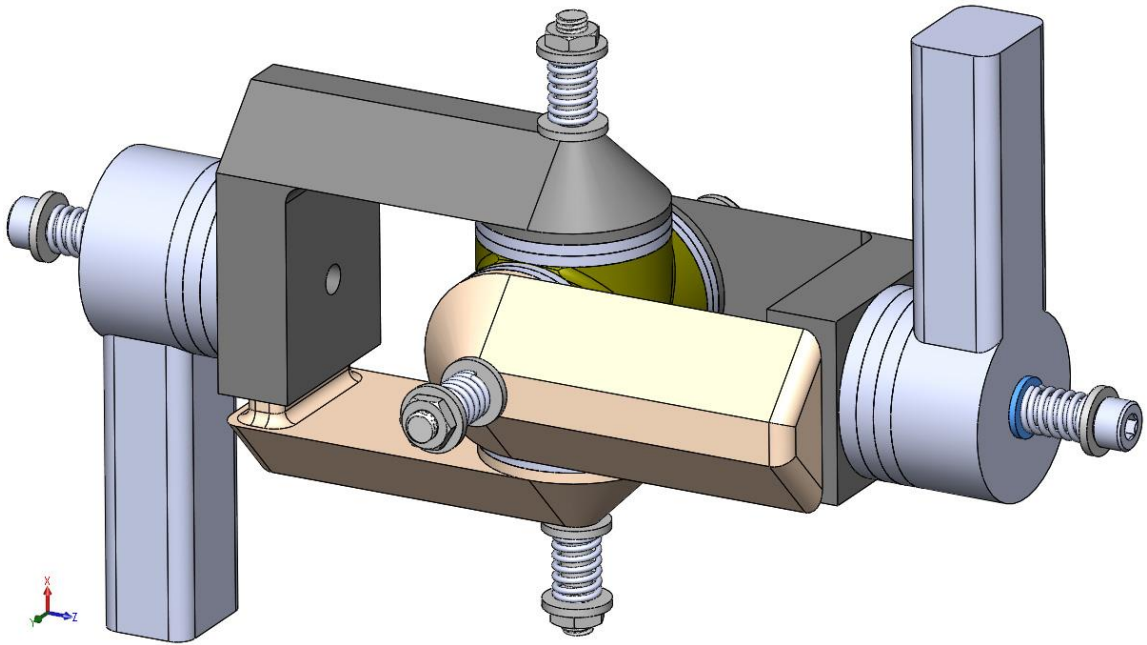


Figure 9-3 A larger view of the ball joint with extended fork parts (RUR)

9.2. Manufacturing

The ball joint (UR or RUR) using sleeves was not fabricated in the machine shop at Memorial University for a lack of time.

As it can be seen from the previous design section, the construction would only require not more effort than making one Universal joint and then two revolute joint. The difficulty levels are similar. The fork parts still remain unchanged and completely interchangeable. The third joint cone is located at one end of the Universal joint making sure that the rotation axis intersects the Universal joint rotation center.

This design also maintains the important interchangeability criteria which is simplifying construction with a lesser number of part types by repeating them. More repeated parts cost less to design and produce than a larger number of different parts. Again, it is easy to assemble and disassemble the ball joint by unscrewing the joint screws simplifying maintenance over traditional fork joints. Added complexity in construction is compensated by maintenance simplification.

Chapter 10

Chapter 10: Conclusion

10.1. Conclusion

The first part was to modify an existing snow crab model in order to include the crab leg joints. It was studied how to provide for those joint models including Fork ball joint, Revolute joint and the combination of Revolute and ball joint to recreate similarity in joint motion.

The fully articulated snow crab was designed and fabricated with all the details utilizing two different techniques of rapid prototyping and manufacturing, namely SLS and FDM. There were some valuable achievements from that work such as:

- The introduction of rigidity of the revolute joint model families to improve the quality of the joints in the crab.
- Different joints such as the revolute joint, ball joint and a combination of them were designed and fabricated in such a way that the motion of the real crab caused by its tendon is simulated by the appropriate use of friction.
- The snow crab models were prepared in two sizes (1:1 and 0.7:1) to allow for robot manipulation tests for robot design purposes as the real dead crabs would become a health hazard.

- Good training for designing a revolute joint, fork revolute joint, universal joint and ball joint with a novel concept.

Then, the second part consisted in the revolute joint design for its application in robot and mechanism designs. The revolute joint was designed with specific criteria which were met. These results were including self-centering and self-aligning, minimizing friction, removing backlash and maximizing rigidity. The revolute joint was successfully designed and fabricated. The features of the revolute joint are conical shape with the 45 degrees taper angle as an optimum design; two sleeves are used in-between the two joint parts with Moly as the dry coating lubricant. The geometrical shape was determined as the first design step. The geometric parameters such as lengths, diameters, angles can be adjusted since they are variable. However, it has been demonstrated how the conical taper angle α plays a key role since its amount directly affects the rotational friction and transmitted torque.

Implementing the rotational joint parts which are attached throughout the contact surfaces, significantly reduces the stress on the contact area compared to the similar ball bearings or roller bearings while it keeps the friction low with using dry lubricant (Moly) in the form of one, two or even three sleeves. The joints can also be constructed without any sleeve. The amount of frictions was determined for the three cases and results compared indicating that two sleeves lead to very good results.

The spring fastens the joint. This allows to adjust friction levels to resist joint separation while trying to keep friction minimal thereby transmitted torque minimal.

In addition, the proposed design met the self-centering factor, which solves the backlash problem at the same time. The revolute joint is therefore capable to accept wear and readjust accordingly. Furthermore, using Moly creates smooth contact surfaces after a period of time and results in zero-clearance approach as one of the desired factors of our joints. Finally, the sleeves can function as a mechanical fuse and if the revolute joint contact surfaces fail, the set of sleeves will be replaced instead of changing the whole joint, which is more cost-effective. More generally, after any operational wear, the sleeves can easily be replaced.

Maintenance on revolute where the joint is disassembled then involves a delicate process of removing the bearing and this can be quite difficult. In the case of the proposed revolute joints, disassembly only requires the removal of one spring thereby providing a simpler solution.

The weight ratio method, among different methods of friction measurement, was chosen to define the rotational transmitted torque, the coefficient of static friction (μ_s) and friction force before coating Moly and after that. The result shows the practical effect of utilizing dry lubricant while the μ_s significantly decreased from 0.1111 in mirror finish stainless steel to 0.0712 after coating the joint surfaces with Moly.

The other joints including the fork revolute joint, the universal joint and the ball joint were designed based on the concept of the revolute joint to meet the criteria and the first two joint were successfully fabricated. Besides the general criteria, the fork revolute joint has more stable function against the axial loads. The ball joint can reach a large range of motion as well as providing for complete ball-retention.

10.2. Future Work

The authors suggest the following functional tests to evaluate and further study the tenure of the current design:

- Measuring the wear over time and rate of wear

Wear can be measured by the weight loss per unit axial projected area and rate of wear can be measured by the weight loss against running time.

- Evaluate fatigue tests

Fatigue can be measured with cyclic loads both in elastic and plastic ranges of the materials used. The tests will also aim to evaluate the changes of material properties lower time.

References

- [1] CNC Cylindrical Grinders, OKUMA,
http://www.okuma.co.jp/english/product/new/gpw_gaw/
- [2] Tsai, L. W. (2000). *Mechanism design: enumeration of kinematic structures according to function*. CRC press.
- [3] Tsai, L. W. (1999). *Robot analysis: the mechanics of serial and parallel manipulators*. John Wiley & Sons.
- [4] Todd, D. J. (Ed.). (2012). *Fundamentals of robot technology: An introduction to industrial robots, teleoperators and robot vehicles*. Springer Science & Business Media.
- [5] UK Patent No 2006, London. 1794. "Iron ball bearings for carriage wheel-axles"
- [6] Suriray, (1873), "Perfectionnements dans les vélocipèdes" (Improvements in bicycles), French patent no. 86,680, issued: August 2, 1869, *Bulletin des lois de la République française*, series 12, vol. 6, page 647.
- [7] Manegold, K-H and FAG Kugelfischer. (1983). *FAG: 1883 - 1983; 100 Jahre industrielle Kugelfertigung, 100 Jahre Wälzlagerindustrie*, Schweinfurt FAG.
- [8] Wingquist, S. (1907). Multi-row self-aligning radial ball bearing. *Swedish patent No. 25406*.

- [9] MICHELL, A. G. M. (1926). Thrust-bearing and like machine element. *U.S. Patent US1602117 A*.
- [10] Bouyer, J., & Fillon, M. (2011). Experimental measurement of the friction torque on hydrodynamic plain journal bearings during start-up. *Tribology International*, 44(7), 772-781.
- [11] Yan, S., Xiang, W., & Zhang, L. (2015). A comprehensive model for 3D revolute joints with clearances in mechanical systems. *Nonlinear Dynamics*, 80(1-2), 309-328.
- [12] Flores, P., & Ambrósio, J. (2004). Revolute joints with clearance in multibody systems. *Computers & structures*, 82(17), 1359-1369.
- [13] Flores, P., Ambrósio, J., & Claro, J. P. (2004). Dynamic analysis for planar multibody mechanical systems with lubricated joints. *Multibody System Dynamics*, 12(1), 47-74.
- [14] Tian, Q., Liu, C., Machado, M., & Flores, P. (2011). A new model for dry and lubricated cylindrical joints with clearance in spatial flexible multibody systems. *Nonlinear Dynamics*, 64(1-2), 25-47.
- [15] Bai, Z. F., & Zhao, Y. (2013). A hybrid contact force model of revolute joint with clearance for planar mechanical systems. *International Journal of Non-Linear Mechanics*, 48, 15-36.
- [16] Yonemoto, K., Takeda, Y., Tong, Z., & Higuchi, M. (2012). A new flexure revolute joint with leaf springs and its application to large workspace parallel robot. *Journal of Advanced Mechanical Design, Systems, and Manufacturing*, 6(1), 76-87.

- [17] Brutti, C., Coglitore, G., & Valentini, P. P. (2011). Modeling 3D revolute joint with clearance and contact stiffness. *Nonlinear dynamics*, 66(4), 531-548.
- [18] Rajput, R. K. (2007). *A text book of automobile engineering*. Firewall Media.
- [19] Cardano, H. (1663). *Opera Omnia, tome X opuscula miscellanea ex fragmentis et paralipomenis*, p. 488–489.
- [20] Dodge, A. Y. (1940). Bearing loads due to universal joint action. *Automotive Industries*, 83, 636-639.
- [21] Evernden, H. I. F. (1949), in *Proceedings of the Institute of Mechanical Engineers, Automotive Division, Part III*, pp. 100-110.
- [22] Yang, A. T., & Freudenstein, F. (1964). Application of dual-number quaternion algebra to the analysis of spatial mechanisms. *Journal of Applied Mechanics*, 31(2), 300-308.
- [23] Fischer, I. S., & Freudenstein, F. (1984). Internal force and moment transmission in a cardan joint with manufacturing tolerances. *Journal of Mechanisms, Transmissions, and Automation in Design*, 106(3), 301-311.
- [24] Gough, V. E., & Whitehall, S. G. (1962, May). Universal tyre test machine. In Proc. FISITA 9th Int. Technical Congress (pp. 117-137).
- [25] Wagner, E. R. (1979). *Universal Joint and Driveshaft Design Manual: Advanced in Engineering. Series No. 7. Society of Automotive Engineers, Inc.. Warrendale, Pennsylvania.*

- [26] Shigley, J. E., & Mischke, C. R. (1986). *Standard handbook of machine design*, McGraw-Hill.
- [27] Lenarcic, J., Bajd, T., & Stanišić, M. M. (2012). *Robot mechanisms* (Vol. 60). Springer Science & Business Media.
- [28] Spherical, Mathworks,
<https://www.mathworks.com/help/phymod/sm/mech/ref/spherical.html?requestedDoMain=www.mathworks.com>
- [29] Faudi, F. (1922). Ball joint, in particular for the steering system of motor vehicles. *German patent No. DE 364495 C*.
- [30] Preben W, J. (1972). Rolling joint mechanisms. *U.S. Patent US 3696683 A*.
- [31] Knuckle Joints Toolless Type Spring Pin for Knuckle only, NJUPS,
<http://in.misumi-ec.com/asia/ItemDetail/10300352310.html>
- [32] Special Materials, Curtis Universal Joint Company,
<https://curtisuniversal.com/products/special-materials/>
- [33] ABOUT MOOG COMPANY, <http://www.moogparts.eu/about-us.html>
- [34] Domed cover plate design, MOOG Company,
www.moogparts.com/pdf/.../english/MOOG_PS_Bulletin_27018_Cover_Plate_En.pdf

- [35] Ball Joints, MOOG Company, http://www.federalmogulmp.com/en-US/Original-Equipment/Brands/MOOG/Pages/Products-By-Category.aspx?BrandId=41&SubCategoryId=53#.V_KZcfkrKUk
- [36] Federal-Mogul Introduces High-Strength Ball Joint, Federal-Mogul Motorparts, <http://www.autoserviceprofessional.com/article/95611/federal-mogul-introduces-high-strength-ball-joint>
- [37] Ball joints tailored to bring strength and convenience, MOOG Company
<http://www.moogproducts.com/en-global/Suspension/Pages/Ball-Joints.aspx>
- [38] SRJointtest, Myostat Motion Control Inc, <http://www.myostat.ca/SRJointtest>
- [39] UNIVERSAL JOINTS, T.A. Kayser, <http://www.sdp-si.com/catalogs/D757-Couplings-Universal-Joints3.php>
- [40] Taghirad, H. D. (2013). *Parallel robots: mechanics and control*. CRC press.
- [41] Jazar, R. N. (2010). *Theory of applied robotics: kinematics, dynamics, and control*. Springer Science & Business Media.
- [42] Patel, Y. D., & George, P. M. (2012). Parallel manipulators applications—a survey. *Modern Mechanical Engineering*, 2(03), 57-64.
- [43] Simaan, N., & Shoham, M. (2000, September). Robot construction for surgical applications. In *The First IFAC Conference on Mechatronic Systems, Darmstadt, Germany*, pp. 553-558.

- [44] Wu, Y., Fu, Z., Xu, J. N., Yan, W. X., Liu, W. H., & Zhao, Y. Z. (2015, August). Kinematic Analysis of 5-DOF Hybrid Parallel Robot. In *International Conference on Intelligent Robotics and Applications* (pp. 153-163). Springer International Publishing.
- [45] Nabat, V., de la O RODRIGUEZ, M., Company, O., Krut, S., & Pierrot, F. (2005, August). Par4: very high speed parallel robot for pick-and-place. In *2005 IEEE/RSJ International conference on intelligent robots and systems* (pp. 553-558). IEEE.
- [46] Bell, C. (2015). Introduction to Delta 3D Printers. In *3D Printing with Delta Printers* (pp. 1-37). Apress.
- [47] Parallel Robot (Delta Robot): Adept Quattro s650H, OMRON ADEPT TECHNOLOGIES, INC, <http://www.adept.com/products/robots/parallel/quattro-s650h/general>
- [48] Williams, R. L., & Joshi, A. R. (1999, December). Planar parallel 3-RPR manipulator. In *Proceedings of the Sixth Conference on Applied Mechanisms and Robotics* (pp. 12-15).
- [49] https://en.wikipedia.org/wiki/Stewart_platform
- [50] Merlet, J. P. (2006). *Parallel robots* (Vol. 128). Springer Science & Business Media.
- [51] Dombre, E., & Khalil, W. (Eds.). (2013). *Robot manipulators: modeling, performance analysis and control*. John Wiley & Sons.
- [52] Briot, S., & Bonev, I. (2007). Are parallel robots more accurate than serial robots?. *CSME Transactions*, 31(4), 445-456.

- [53] ROBOTIQ, Ahmed Joubair (Eng. Ph.D.), <http://blog.robotiq.com/bid/72831/What-are-the-Sources-of-Robot-Inaccuracy>
- [54] Cui, H., & Zhu, Z. (2006). Error Modeling and Accuracy of Parallel Industrial Robots. *Industrial Robotics*, 573.
- [55] Andeen, G. (1989). Design differences between robotic manipulators and construction equipment. In Proc. 6th Int. Symp. on Automation and Robotics in Construction (pp. 253-259). Construction Industry Institute.
- [56] Manufacturing Process Comparison chart, Sculpteo Co.,
<https://www.sculpteo.com/en/3d-printing/3d-printing-and-traditional-manufacturing-processes/>
- [57] Phillips, S. D., & Bosch, J. A. (1995). Coordinate Measuring Machines and Systems. ed. John A. Bosch, Marcel Dekker, New York.
- [58] Hocken, R. J., & Pereira, P. H. (Eds.). (2016). *Coordinate measuring machines and systems*. CRC Press.
- [59] Sładek, J. A. (2016). *Coordinate Metrology*. Springer.
- [60] Gibson, I., Rosen, D., & Stucker, B. (2014). *Additive manufacturing technologies: 3D printing, rapid prototyping, and direct digital manufacturing*. Springer.
- [61] 3D Printing, CustomPartNet Inc, <http://www.custompartnet.com/wu/3d-printing>
- [62] FDM, CustomPartNet Inc, <http://www.custompartnet.com/wu/fused-deposition-modeling>

- [63] Kai, C. C., Fai, L. K., & Chu-Sing, L. (2010). *Rapid prototyping: principles and applications in manufacturing*. World Scientific Publishing Co., Inc.
- [64] Bártolo, P. J. (Ed.). (2011). *Stereolithography: materials, processes and applications*. Springer Science & Business Media.
- [65] Stereolithography, CustomPartNet Inc,
<http://www.custompartnet.com/wu/stereolithography>
- [66] Gu, D. (2015). *Laser additive manufacturing of high-performance materials*. Springer.
- [67] SLS, CustomPartNet Inc, <http://www.custompartnet.com/wu/selective-laser-sintering>
- [68] SNOW CRAB – A CHARMING DELICACY, PucciFoods,
<http://puccifoods.com/pucciseafood-new/snow-crab-charming-delicacy/>
- [69] Leonesio, M., Bianchi, G., & Manara, P. (2007, June). A general approach for self-locking analysis in closed kinematic chains. In *Proceedings of the 12th World Congress in Mechanism and Machine Theory* (pp. 141-147). Besancon France.
- [70] Xu, B., Dong, P., Zhang, J., Liu, M., & Yao, J. (2014). Design and Evaluation of a Novel Self-Locking Quick Release Mechanism Featured by Heavy Load, Fast Response, and High Security. *Advances in Mechanical Engineering*, 2014(2), 1-16.
- [71] Olędzki, A. A. (1995). Modeling and simulation of self-locking drives. *Mechanism and machine theory*, 30(6), 929-942.

- [72] Leonesio, M., & Bianchi, G. (2009). Self-locking analysis in closed kinematic chains. *Mechanism and Machine Theory*, 44(11), 2038-2052.
- [73] Fauroux, J. C., & Morillon, J. (2010). Design of a climbing robot for cylindro-conic poles based on rolling self-locking. *Industrial Robot: An International Journal*, 37(3), 287-292.
- [74] Qiao, J., Shang, J., & Goldenberg, A. (2013). Development of inchworm in-pipe robot based on self-locking mechanism. *IEEE/ASME Transactions On Mechatronics*, 18(2), 799-806.
- [75] Hoffait, S., Brüls, O., Granville, D., Cugnon, F., & Kerschen, G. (2010). Dynamic analysis of the self-locking phenomenon in tape-spring hinges. *Acta Astronautica*, 66(7), 1125-1132.
- [76] Lansdown, A. R. (1999). *Molybdenum disulphide lubrication* (Vol. 35). Elsevier.
- [77] Amaro, R. I., Martins, R. C., Seabra, J. O., Renevier, N. M., & Teer, D. G. (2005). Molybdenum disulphide/titanium low friction coating for gears application. *Tribology International*, 38(4), 423-434.
- [78] Muratore, C., & Voevodin, A. A. (2006). Molybdenum disulfide as a lubricant and catalyst in adaptive nanocomposite coatings. *Surface and coatings technology*, 201(7), 4125-4130.
- [79] Phakatkar, H. G. (2008). *Theory of Machines and Mechanisms*. 4th ed.
- [80] Brar, J. S. (2005). *Theory of Machines*. India. Laxmi Pub.

- [81] Beer, F. P., & Johnston, E. R. (2009). *Vector mechanics for engineers: Statics and dynamics* (9th ed.). New York: McGraw-Hill.
- [82] Ambekar, A. G. (2007). *Mechanism and Machine Theory*, India, PHI Learning Pvt. Ltd.
- [83] Popov, V. (2010). *Contact mechanics and friction: physical principles and applications*. Springer Science & Business Media.
- [84] How to Calculate Conical Taper, Camela Bryan,
http://www.ehow.com/how_6644716_calculate-conical-taper.html
- [85] Lamikiz, A., de Lacalle, L. N. L., & Celaya, A. (2009). Machine tool performance and precision. In *Machine Tools for High Performance Machining* (pp. 219-260). Springer London.
- [86] Font-Llagunes, J. M. (Ed.). (2016). *Multibody Dynamics: Computational Methods and Applications* (Vol. 42). Springer.
- [87] How to measure friction?, Tribology-abc, <http://www.tribology-abc.com/abc/friction.htm>
- [88] Hands On: Stanley Fat Max Xtreme Auto Trigger Clamp, SEAN O'HARA,
<http://toolmonger.com/2007/05/17/hands-on-stanley-fat-max-xtreme-auto-trigger-clamp/>
- [89] Tribometers | Friction and Wear Loss Testing Equipment, LPR Global,
<http://www.uskoreahotlink.com/>

- [90] Modeling Degrees of Freedom, Mathworks,
<http://www.mathworks.com/help/phymod/sm/mech/ug/modeling-degrees-of-freedom.html>
- [91] Seherr-Thoss, H. C., Schmelz, F., & Aucktor, E. (2013). *Universal joints and driveshafts: analysis, design, applications*. Springer Science & Business Media.
- [92] Types of Universal Joints, Beldenuniversal,
<http://www.beldenuniversal.com/products/universal-joints>
- [93] Alexandru, P., Vișa, I., & Alexandru, C. (2014). Modeling the angular capability of the ball joints in a complex mechanism with two degrees of mobility. *Applied Mathematical Modelling*, 38(23), 5456-5470.
- [94] Faghih, M.H. & Rolland, L. (2016, June). Design and Fabrication of a New Revolute Joint Using Dry Lubricant. In *The 4th Joint International Conference on Multibody System Dynamics*. Montréal, Canada.